Element Transport and Partitioning Along Tidal Channels in Southwest Bangladesh

Matthew Dietrich[1] and John Ayers[2]

[1]Indiana University - Purdue University Indianapolis
[2]Vanderbilt University

November 23, 2022

Abstract

Studies of element partitioning between suspended sediment and water with increased seawater mixing are sparse, particularly in Bangladesh. However, these studies are important for understanding elemental cycling, pollutant transport, and impacts on aquaculture and sensitive ecosystems in estuaries and tidal deltas such as the Sundarbans mangrove forest in Southwest Bangladesh. Thus, water samples collected within the upper 1m of the water column along a transect of well-mixed tidal channels in Southwest Bangladesh during the dry season were analyzed for dissolved and suspended sediment element concentrations and other geochemical parameters. While most elements in the suspended load were close to or depleted relative to upper continental crust (UCC), several trace elements such as Sb, As, Cd and Se were slightly enriched. Additionally, most trace elements in the dissolved load were well above world average riverine concentrations, particularly Se and As. Dissolved load Ba and Se displayed mostly conservative mixing trends with seawater. Barium was likely originally sourced from sediment desorption and groundwater exfiltration, while Se may have been anthropogenically sourced from the city of Khulna or farther upstream. Dissolved As did not display conservative mixing trends, and may ultimately be geogenic in origin, possibly from groundwater. Ni and Co show trends consistent with desorption from competitive seawater cation exchange along the transect, similar to a study in the nearby Hooghly Estuary in West Bengal. Collectively, our results show that combined anthropogenic and natural influences on trace element distributions in coastal environments are important to quantify for continual protection of natural areas and better understanding of trace element discharge to global oceans.

ELEMENT TRANSPORT AND PARTITIONING ALONG TIDAL CHANNELS IN SOUTHWEST BANGLADESH

Authors: Matthew Dietrich[a1] and John C. Ayers[a]

[a]Department of Earth and Environmental Sciences, Vanderbilt University, 5726 Stevenson Center, 7th floor, Nashville, TN 37240, United States

[1]Corresponding Author Current E-Mail Address: mjdietri@iu.edu

Abstract:

Studies of element partitioning between suspended sediment and water with increased seawater mixing are sparse, particularly in Bangladesh. However, these studies are important for understanding elemental cycling, pollutant transport, and impacts on aquaculture and sensitive ecosystems in estuaries and tidal deltas such as the Sundarbans mangrove forest in Southwest Bangladesh. Thus, water samples collected within the upper 1m of the water column along a transect of well-mixed tidal channels in Southwest Bangladesh during the dry season were analyzed for dissolved and suspended sediment element concentrations and other geochemical parameters. While most elements in the suspended load were close to or depleted relative to upper continental crust (UCC), several trace elements such as Sb, As, Cd and Se were slightly enriched. Additionally, most trace elements in the dissolved load were well above world average riverine concentrations, particularly Se and As. Dissolved load Ba and Se displayed mostly conservative mixing trends with seawater. Barium was likely originally sourced from sediment desorption and groundwater exfiltration, while Se may have been anthropogenically sourced from the city of Khulna or farther upstream. Dissolved As did not display conservative mixing

trends, and may ultimately be geogenic in origin, possibly from groundwater. Ni and Co show trends consistent with desorption from competitive seawater cation exchange along the transect, similar to a study in the nearby Hooghly Estuary in West Bengal. Collectively, our results show that combined anthropogenic and natural influences on trace element distributions in coastal environments are important to quantify for continual protection of natural areas and better understanding of trace element discharge to global oceans.

Keywords: Estuary mixing; element partitioning; trace metals; suspended sediment transport; Southwest Bangladesh

1 Introduction

Estuarine environments can have important water-particle reactions due to the mixing of upstream freshwater and seawater (e.g., de Souza Machado et al., 2016; Samanta & Dalai, 2018). These interactions are important to quantify because of their profound impacts on the riverine fluxes of both solid-phase and dissolved phase elements to the oceans. Specifically, changes in pH or the influence of seawater ions in an estuarine environment can affect elements through processes such as sorption, flocculation, or ion exchange (e.g., Hatje et al., 2003; Li et al., 1984; Millward & Liu, 2003; Samanta & Dalai, 2018; Thanh-Nho et al., 2018). For example, desorption from suspended sediment due to competitive sorption with Na can increase some element concentrations in the dissolved load and decrease their concentrations in the suspended load (Samanta & Dalai, 2018). Additionally, changes in pH and dissolved oxygen due to seawater mixing can cause certain elements such as Mn to precipitate from solution (Thanh-Nho et al., 2018). Research in estuarine environments throughout the world have shown how changes

in river chemistry with increasing amounts of seawater mixing are often more complex than simple conservative mixing processes (e.g., de Souza Machado et al., 2016; Samanta & Dalai, 2018; Strady et al., 2017; Thanh-Nho et al., 2018), and thus these dynamic environments require thorough investigation.

Although previous work has analyzed geochemical changes in the dissolved and suspended load directly to the west of Bangladesh in the Hooghly Estuary in India (Samanta & Dalai, 2016, 2018), there have been no detailed geochemical examinations of elements in the dissolved and suspended load in Bangladesh rivers during seawater mixing besides Ba and Ra (Carroll et al., 1993; Moore, 1997). The Hooghly Estuary experiences similar hydrodynamics as the tidally influenced rivers in Southwest Bangladesh, with large tidal influence and drastic differences in seasonal discharge, but experiences greater anthropogenic influence closer to the mouth of the river from cities such as Kolkata and Haldia (Jayaram et al., 2021). It is imperative to quantify and understand geochemical changes in Bangladesh rivers because of increasing anthropogenic influence, not only for improving general knowledge of riverine-ocean elemental fluxes and elemental cycling within global estuaries, but because potentially harmful metals such as Ni and Co may have increased mobility in some pristine estuary environments due to competition with seawater cations for adsorption (e.g., Millward & Liu, 2003; Samanta & Dalai, 2018). Coastal Bangladesh is an ideal natural laboratory for these detailed geochemical investigations because of the large influx of sediment, abundance of river tributaries, and tidal influence from the ocean. It is also analogous to other deltaic systems throughout the world, such as the Mississippi River or Niger River deltas (e.g., Lindsay et al., 1991), making research findings here relevant to other coastal settings.

Bangladesh lies between India and Myanmar (Burma), with the Bay of Bengal along its southern coastline (Fig. 1). Bangladesh mostly sits in a low-elevation deltaic environment, filled with alluvial deposits from the Himalayas carried by the Ganges and Brahmaputra (G-B) rivers, and experiences a strong seasonal monsoon climate, with about 80% of annual rainfall occurring between the months of June to September (Chowdhury, 2010). This strong seasonality leads to large differences in surface water chemistry in coastal areas, with tidally-influenced rivers experiencing vastly lower levels of salinity during the monsoon season compared to the drier months (e.g., Akter & Ahmed, 2019; Ayers et al., 2017).

Southwest Bangladesh (Fig. 1) is in a tidal delta and its tributaries stem from the Ganges River, originating in the western Himalayas. These river tributaries experience a large inundation of seawater during the dry season with the tidal influence extending just north past Khulna (e.g., Brammer, 2014), and are hereafter called tidal channels. These tidal channels experience semi-diurnal tides (Hale et al., 2019) and in the wet season tidal channel discharges encounter highly saline waters near the coast, although the salinity front extends much less inland compared to the dry season. Tidal cycle influence on water composition in the dry season in Southwest Bangladesh tends to be relatively minimal, with salinity in the dry season often changing ~1ppt or less between high and low tide in Sundarbans tidal channels near our study area (S. M. Rahaman et al., 2014; S. M. B. Rahaman et al., 2013).

Hale et al. 2019 extensively examined the properties of several tidal channels in this region. They found that one of the larger tidal channels sampled in our study, the Shibsa, has widths of ~1-2 km and depths up to 20m in some locations, while one of the smaller tidal

channels in our study, the Bhadra, only has widths of 0.15–0.3 km. The differences between the larger (e.g., Rupsha and Shibsa rivers) and smaller channels (e.g., Bhairab and Bhadra rivers) in our study has an important influence on suspended sediment loads, for even though tidal channels in the region generally contain more suspended sediment and greater suspended sediment concentrations in the wet season than the dry season, smaller channels experience more seasonality in suspended sediment concentrations compared to larger channels whose sediment loads are predominantly influenced by tidal variability. Most of the water exchanged through the tidal channels in this area is tidally reworked, with estimates suggesting that within our study area in the Shibsa River, nearly 2×10^{11} m^3 of water is moved through the channel each year (Hale et al., 2019).

Southwest Bangladesh also contains the largest mangrove forest in the world, the Sundarbans (dark green in southern extent of Fig. 1), which is susceptible and sensitive to anthropogenic pollution (e.g., Ahmed et al., 2011; Kumar et al., 2016). A potential anthropogenic pollutant source upstream of the Sundarbans is the city of Khulna along the Bhairab and Rupsha rivers, which is the third most populated urban center in Bangladesh with ~1.5 million people (e.g., Datta et al., 2020). Khulna holds several industrial and municipal sources that may contribute effluent discharge to the surrounding rivers, such as oil refineries, power companies, and jute mills (Kibria et al., 2016).

This study aims to utilize measured data of the suspended and dissolved loads from a tidal channel transect (Bhairab-Rupsha-Bhadra-Shibsa rivers) in Southwest Bangladesh (Fig. 1) to examine geochemical changes with increasing seawater mixing along the transect (Fig. 2), as

well as identify whether any toxic elements (i.e., Se and As) that may prove hazardous to the Sundarbans/rural agricultural areas are sourced from the city of Khulna. Of focus are Ba, Ni and Co because of previous research of these elements near the study area (Carroll et al., 1993; Moore, 1997; Samanta & Dalai, 2016, 2018), as well as As and Se because of the relatively limited research of these potentially toxic elements in Southwest Bangladesh surface waters (Ayers et al., 2017; Dietrich & Ayers, 2021b). Hypothesized mechanisms affecting elements in the solid and dissolved loads are desorption, conservative seawater mixing, mineral dissolution, and ion-exchange. Characterizing the geochemical processes within the tidal channels will give important insights into elemental cycling and mobilization that can be applied to other estuaries around the world, particularly pristine ecosystems that may be exposed to increased inputs from anthropogenic perturbations upstream.

2 Methods

2.1 Sample collection

Water samples from the upper 1m of the water column were collected in metal (samples MD-TC-14 and MD-TC-15) and plastic buckets that were rinsed between samples, which then filled 1L plastic HDPE bottles (with minimal headspace and with the bucket water well mixed to prevent sediment settling). No anomalous metal(loid) concentrations in the metal bucket samples were detected besides elevated dissolved Si in MD-TC-14 (Fig. B1). Samples were taken from the upper 1m of the water profile because this portion of the water column is representative of the slow-settling suspended sediment load being deposited into aquaculture ponds within the

study area, and thus of greatest health relevance. Additionally, sampling in the upper portion of the water column is much easier logistically, although future water/sediment sampling at various depths in the water column would be useful, since the composition and mineralogy of suspended sediments are known to change dramatically with depth (e.g., Garzanti et al., 2011). Buckets were rinsed in-between each sample. Filtering of the samples was not performed in the field. Attempts were made to ensure representative samples, with samples taken from a boat near mid-channel where river flow was constant and not stagnant. Samples were collected at the end of the dry season in May, 2019 as support for another paired study (Dietrich and Ayers, 2021a) because of the predominant use of tidal channels in the area for saltwater aquaculture irrigation at this time (e.g., Ayers et al., 2017). Samples were refrigerated upon return to Vanderbilt University and stored at room temperature during transport.

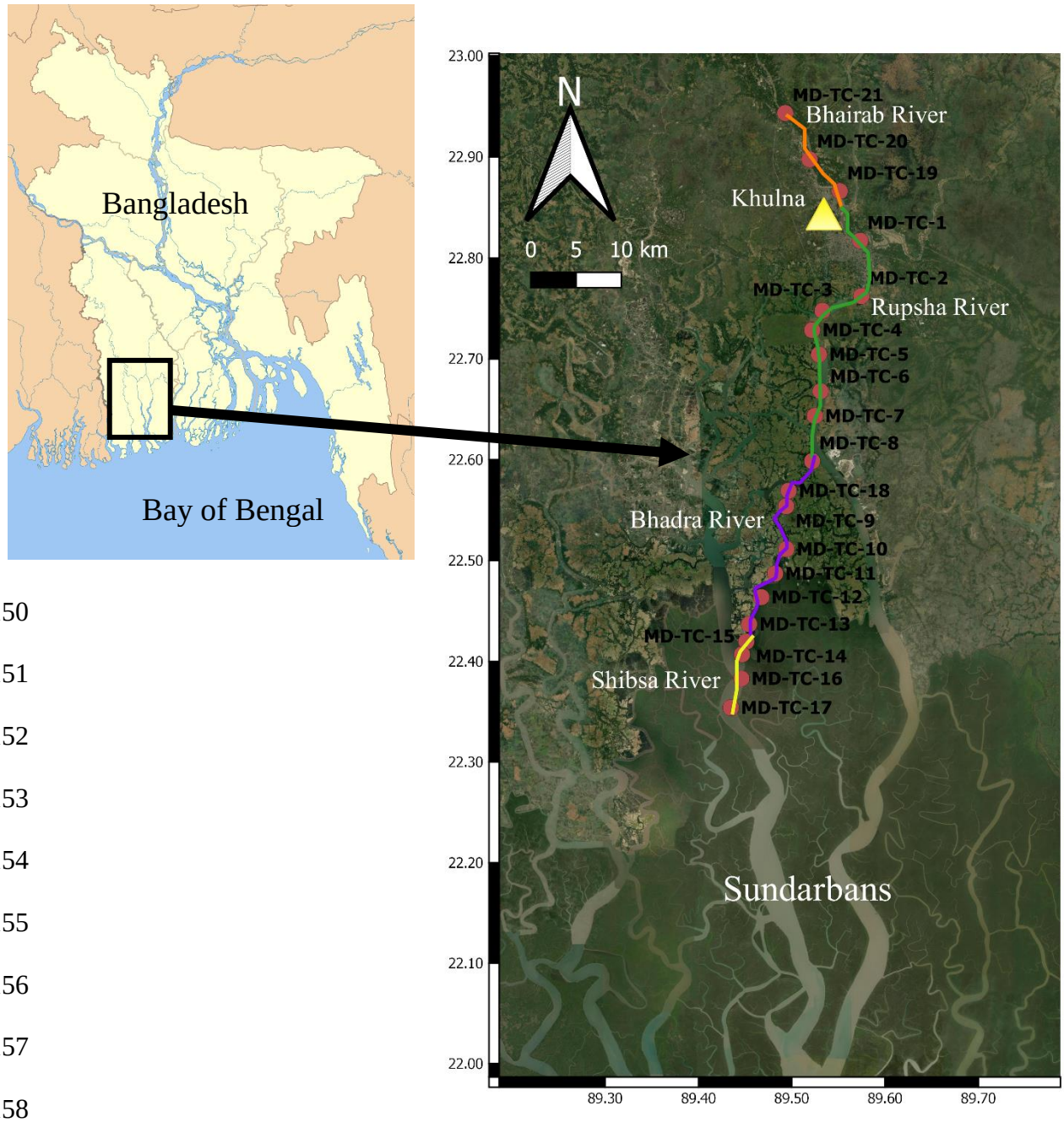

Figure 1: Map of the sample sites along the tidal channel transect (Bhairab-Rupsha-Bhadra-Shibsa as the main rivers) in Southwest Bangladesh, with the triangle representing the city of Khulna. The Sundarbans (natural mangrove forest) is the dark green area to the south of the sample locations. The Bay of Bengal is to the south of the Sundarbans. The colored lines along

the transect represent the main channels sampled from N-S as: Bhairab (orange), Rupsha (green), Bhadra (purple), and Shibsa (yellow).

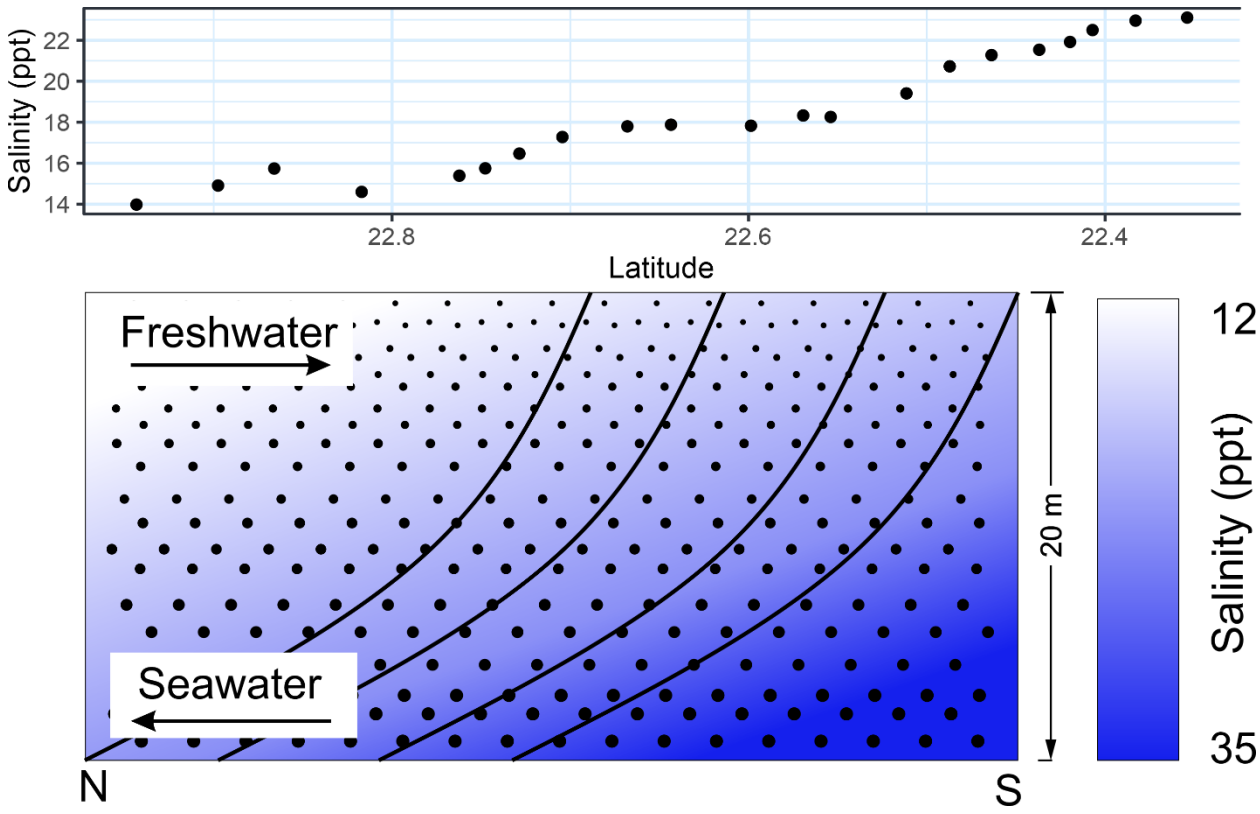

Figure 2: Conceptual diagram of seawater mixing along the river transect. The proportion of seawater in the tidal channel increases to the south. Solid black lines represent velocity profiles within the water column, and black dots represent suspended sediment. Above the conceptual diagram is a graph of in situ measured salinity along the transect.

2.2 Field measurements

A Hach Hydrolab DS5 was used to gather in situ surface water measurements of pH, oxidation-reduction potential (ORP), turbidity (NTU), salinity (ppt), Eh in millivolts (mV), and specific conductivity (SpC) in microsiemens per centimeter (µS/cm) for all water samples. After sampling from the upper 1m of the water column with the bucket, the Hydrolab DS5 plastic sensor cover was filled about 80% after rinsing in-between samples, with the Hydrolab sensors then immersed into the water. For accurate turbidity measurements, the Hydrolab was filled before sediment settling could significantly occur in the bucket. However, turbidity would decline during the measurement because of sediment settling around the Hydrolab sensors. Calibration of the Hydrolab DS5 was performed before field use for ORP, pH, turbidity, and SpC with standard calibration solutions. In-situ ORP measurements are intended for differentiating between oxic versus anoxic conditions instead of quantifying specific values, such as described in Ayers et al. (2016, 2017). ORP (relative to the Ag/AgCl redox couple) was converted to Eh (relative to the standard hydrogen electrode (SHE)) in Supplementary Table 1 by adding 187 mV to each field measurement. GPS coordinates were also recorded at each sample site and are listed in Supplementary Table 1.

2.3 Sample analyses

2.3.1 Water/solid sample prep

Water samples were filtered with a 2.5 µm Whatman® ashless paper filter via a vacuum-suction device to collect the suspended sediment following refrigerated storage at Vanderbilt

University (days from sampling to filtration shown in Supplementary Table 1). Although the filter size was 2.5 µm, additional smaller particles were likely captured through cohesion of silty clay particles. Following filtration at 2.5 µm, a homogenized and well-mixed subset of each sample was filtered at 0.2 µm with a Nalgene Polyvinylidene Fluoride (PVDF) filter. 2mL of the 0.2 µm filtered samples were acidified with a drop of HNO_3 and diluted with deionized water to achieve a 5:1 dilution for inductively coupled plasma analyses (ICP-MS and ICP-OES). A 10:1 dilution was performed for a reanalysis of Na on the ICP-OES. A 20-30mL subset of the filtered undiluted water samples were used for ion chromatography (IC) and total organic carbon (TOC) analysis.

The filter paper full of the suspended sediment was dried overnight at ~45-50ºC following filtration. The filter and suspended sediment were then weighed to determine suspended sediment concentrations (SSC) from ~1L of the water that was filtered (to prevent headspace, slightly more than 1L of water filled each bottle that was filtered). The weight of the filter paper (weighed after drying at ~45-50ºC overnight before filtering the water sample) was subtracted from the dried filter + suspended sediment weight to determine SSC. Because sediment was uniformly distributed across the filter paper, splits between 0.25-0.5 grams of the filter paper + sediment were prepared for acid digestion.

2.3.2 Water sample analyses

All 5:1 diluted and acidified water samples were analyzed on a Perkin Elmer NexION 2000B ICP-MS in both standard and kinetic energy discrimination (KED) modes using EPA

Method 6020B at Vanderbilt University for the elements As, Be, Cd, Co, Cr, Cu, Fe, Mn, Mo, Ni, Pb, Sb, Se, Ti, Tl, V, and Zn. All acidified surface water samples were also analyzed on an Agilent 5110 VDV ICP-OES using EPA Method 6010D at Vanderbilt University to report the ions: Al, As, B, Ba, Ca, Fe, K, Mg, Na, P, S, Si, and Sr. A rerun for Na at a 10:1 dilution was performed for the ICP-OES because of elevated Na concentrations from seawater mixing. Essentially, the same ICP methods were employed in previous investigations by the authors (Ayers et al., 2017; Dietrich & Ayers, 2021b). All filtered, unacidified surface water samples were analyzed for inorganic and organic carbon content via a Shimadzu model TOC-LCPH using EPA Method 9060A. Unacidified water samples were also analyzed for Cl, F, Br, NO_3, PO_4, and SO_4 with a Metrohm 881 Compact IC Pro using SW-846 EPA Method 9056. F, NO_3 and PO_4 were routinely below detection limit and thus not reported. The elements Fe and As are reported from the ICP-MS instead of ICP-OES, because of improved precision on the ICP-MS for these elements due to lower detection limits compared to the ICP-OES. Method detection limits (MDLs) are listed in Supplementary Table 2.

2.3.3 Solid sample analysis

0.25-0.5 grams of each filter paper + suspended sediment subsample were digested according to EPA Method 3051A at The Ohio State University Service Testing and Research Laboratory (STAR Lab) for analysis on an Agilent 5110 ICP-OES for the elements: Al, As, B, Ba, Be, Ca, Cd, Co, Cr, Cu, Fe, K, Li, Mg, Mn, Mo, Na, Ni, P, Pb, S, Sb, Se, Si, Sr, Tl, V and Zn. It is noted that EPA Method 3051A does not lead to complete digestion of silica, and thus Si was excluded in the reported values. NIST standards 1646a (estuarine sediment) and 2702

(inorganics in marine sediment) were run in duplicate to assess element percent recovery for certified and reference mass fraction values from each standard using EPA Method 3051A and the ICP-OES at STAR Lab in a separate analytical run from suspended sediment samples (Table B1). While recovery for elements in silicate minerals (i.e., Al and Si) and elements typically in more resistant minerals such as feldspars was poor (i.e., K and Na), most trace elements displayed recovery typically between ~80-120% (i.e., As, Cu, Ni, Zn, Sb, Co). Additionally, as this study was largely focused on elemental trends and correlations, percent recovery is less important as long as analyses were consistent, especially because we were interested on the elemental fraction that was more likely to exchange between sediment and tidal channel water (i.e., weak HNO_3 acid digestion in EPA Method 3051A).

Suspended sediment element concentrations were estimated using the "suspended sediment concentration factor," determined from the (blank filter + suspended sediment mass)/suspended sediment mass. This assumed a uniform ratio of suspended sediment distributed over the filters, which was observed consistently. This concentration factor was multiplied by the measured sediment-element concentrations to account for the weight dilution of the filter paper (filter paper element concentrations determined by running blanks are all very low (Supplementary Table 3), but take up a significant mass comparable to the sample and are mainly comprised of unanalyzed elements such as C, O and H). The filter paper and suspended sediment digestion and filtering methods are similar to previous studies (Wang & Wang, 2016; Weng & Wang, 2014), although the concentration dilution from the filter paper is explicitly described/addressed in this study. Approximate MDLs based on a 200x dilution factor for solid sample acid digestion are listed in Supplementary Table 3.

2.3.4 Transmission electron microscopy (TEM)

A droplet from one unfiltered tidal channel sample taken in the upper 1m of the water column in the study area (P32-TC; Dietrich & Ayers, 2021b) was mounted via drop-casting suspension on a lacey carbon-coated copper TEM grid, dried, then analyzed on a Tecnai Osiris equipped with SuperX quad EDS detectors with an accelerating voltage of 200kV. Suspended sediment from samples MD-TC-7 and MD-TC-11 were also analyzed on the Tecnai Osiris TEM after removing the sediment from the filter paper, mixing with isopropanol, sonicating for about 2 minutes, then placing a drop onto a carbon-coated copper TEM grid and wicking away the excess solvent. TEM and STEM-EDS maps were generated to characterize solid particulates that are present in tidal channel water, with STEM-EDS maps drift corrected with Bruker Esprit version 1.9 with a beam current of approximately 1nA. Wt. and at. % element quantification based on EDS spectra was performed using standardless cliff Lorimer approximation. TEM work was performed at the Vanderbilt Institute of Nanoscale Science and Engineering (VINSE).

2.3.5 Grain size analysis

A duplicate, unfiltered water sample of MD-TC-21 was analyzed for particle size via laser granulometry with a Malvern Mastersizer 2000 at Vanderbilt University. Most of the homogenized sample filled a 1L beaker after running deionized water through the instrument to establish background concentrations. The sample was then deflocculated via sonication before analysis. A homogenized subset of dried, filtered (>2.5µm) suspended sediment from several representative samples (including a replicate sample) along the transect were mixed in a 1L

beaker of water using the same procedures as above, but with a Malvern Mastersizer 3000 at Vanderbilt University.

2.3.6 Powder X-ray diffraction (XRD)

Dried, homogenized powder samples of suspended sediment from sample MD-TC-18 and deposited sediment adjacent to shrimp pond (sample site KA-4; Dietrich & Ayers, 2021b) were dry cast on 20 x 20mm square sample glass holders with a 0.2mm indent. The samples were then analyzed with a Rigaku SmartLab powder X-ray diffractometer at Vanderbilt University with a Cu Kα (lambda = 0.154 nm) source at 40 kV and 44 mA. The detector was a D/teX Ultra 250 1D silicon strip detector. PDXL software identified the mineral phases associated with the intensity peaks.

2.4 Quality control

Samples were refrigerated upon arrival to Vanderbilt University, although it is noted that ~1-2 weeks of time passed without refrigeration of samples. Additionally, a significant amount of time passed between sampling and filtration. Thus, several checks were made to decipher whether storage time in general had any effect on suspended sediment and dissolved load composition due to element exchange. The days between sampling and filtering are displayed in Supplementary Table 1, and results/discussion of possible element exchange over time between the dissolved load and suspended load within the 1L bottles are addressed in Text B1 and Text B2 (Supporting Information).

Three 1L deionized water blanks were filtered under the same lab methodology as the tidal channel samples at the beginning, middle and end of the sample filtration process (with the same beakers that were cleaned in-between samples) for a total of 3 blanks with 0.2 µm filtered dissolved element concentrations and element concentrations of the filter paper itself. These values were routinely low or below detection limit, with the blanks' concentrations listed in Tables 2 and 3.

Filtered water samples analyzed with the ICP-MS, ICP-OES, IC and TOC analyzers at Vanderbilt University were run with standard solutions and blanks. Standards were required to be within 15% of the known value, while blanks were required to be below the MDL. The geometric mean charge balance error for water samples was approximately 7.7%, slightly higher than the charge balance errors for studies in the area that used similar methods (3.9%, Ayers et al., 2017; 4.6% Dietrich & Ayers, 2021b).

Additionally, duplicate samples that were filtered in the field at 0.45 µm and analyzed for the same water parameters (Dietrich & Ayers, 2021b) as this study were compared to the 1L duplicate subset of water samples filtered in the lab (in this study), for possible discrepancies between methodologies. It is noted that several trace elements such as Cr, Cu, Se, Zn, P, Co and Ni did not match well in several samples, possibly because of differences in filter size/methodology or slight chemical changes during sample storage. See Text B1 (Supporting Information) and Section 4.2.3 for elaboration.

pH and ORP measurements of refrigerated water samples (stored at 4°C, measured at room temperature) were taken in the laboratory approximately five months after sample collection and indicated that redox conditions changed minimally. The arithmetic mean field pH was 7.61 ± 0.09, while the lab pH was 7.49 ± 0.11. Field ORP (non-converted to Eh) was 269.5 ± 9.8 while the lab ORP was 219.9 ± 10.5.

Overall, despite sampling/analytical challenges due to the logistics of our research in a remote coastal environment, contamination of samples should be minimal and post-sampling effects on element concentrations in the dissolved and suspended load should also be relatively minimal, thus not affecting our main data interpretations.

2.5 Data processing

QGIS v.3.10.8 was utilized for map generation and ArcGIS Online was used for watershed maps. RStudio and Microsoft Excel were used for figure generation and statistical analyses. The Geochemist's Workbench 14.0 was used to calculate mineral saturation indices, dissolved HCO_3^- concentrations (from measured dissolved inorganic carbon (DIC)), and charge balance error using the default thermo.dat database (Bethke, 2007). Uncertainties are reported as sample standard deviation (1σ) for all elemental and geochemical results. Final reported element concentrations in the dissolved load from ICP analyses (Supplementary Table 2) are based on the more precise 5.1:1 and 10.2:1 dilutions used, although the 2% difference of rounded values used in figure generation is deemed negligible and less than that of the figure lines/points. Reported Kd values (Table B2) use the original 5:1 and 10:1 dilution because they are log ratio values and

366 the 2% change in dissolved concentrations is often negligible compared to the generally much
367 greater concentrations in the suspended load.
368
369 **3 Results**
370
371 *3.1 Grain size distribution and sediment mineralogy*
372
373 Suspended sediment from an unfiltered duplicate water sample (MD-TC-21 duplicate;
374 upstream in Bhairab River) had a median grain size of 12.2 μm and a volume-weighted mean
375 grain size of 16.0 μm. Approximately 98.6 % of the particle volume was > 2.5 μm. Suspended
376 sediment recovered from 2.5 μm filters for the samples MD-TC-18, MD-TC-5, MD-TC-9, and a
377 replicate of MD-TC-9 (MD-TC-9-Dup) had median grain sizes of 14.8-16.9 μm; with volume-
378 weighted mean grain sizes between 21.3 and 23.3 μm. These samples included both upstream
379 and downstream portions of the transect, as MD-TC-18 and MD-TC-9 were taken >40 km
380 downstream of MD-TC-21 near the confluence of the Bhadra and Dhaki rivers off the Rupsha
381 (MD-TC-9) or within the confluence (MD-TC-18). Their approximate grain size distributions are
382 shown in Fig. 3, which are unimodal and overlap significantly.
383
384 XRD data illustrate several noticeable peaks in the suspended sediment sample (MD-TC-
385 18) and the sediment adjacent to a shrimp pond (Fig. B2). These peaks are associated with
386 minerals such as quartz, muscovite, dolomite, and clay minerals such as chlorite and illite.
387 Qualitatively, the peaks in samples MD-TC-18 and KA-4 are quite similar and overlap
388 significantly (Fig. B2).

3.2 Dissolved and suspended load concentrations and geochemical parameters

Because not all geochemical results follow a normal distribution and are closest to being lognormally distributed, means are reported as geometric means, with variability reported as sample standard deviation. In general, tidal channel samples were near-neutral in pH with very little variation (7.61 ± 0.09) (Supplementary Table 1). Conditions were generally oxidizing based on the positive measured Eh values (456 ± 10 mV), and suspended sediment concentrations (SSC) varied significantly along the tidal channel transect (0.49 ± 0.56 g/L). Water samples were commonly saturated in: K-feldspar, kaolinite, muscovite, dolomite, illite, barite, albite, gibbsite and witherite (Supplementary Table 1). Tidal channel samples have a high salinity of 18 ± 3 ppt, indicative of mixing with seawater from the Bay of Bengal (BoB).

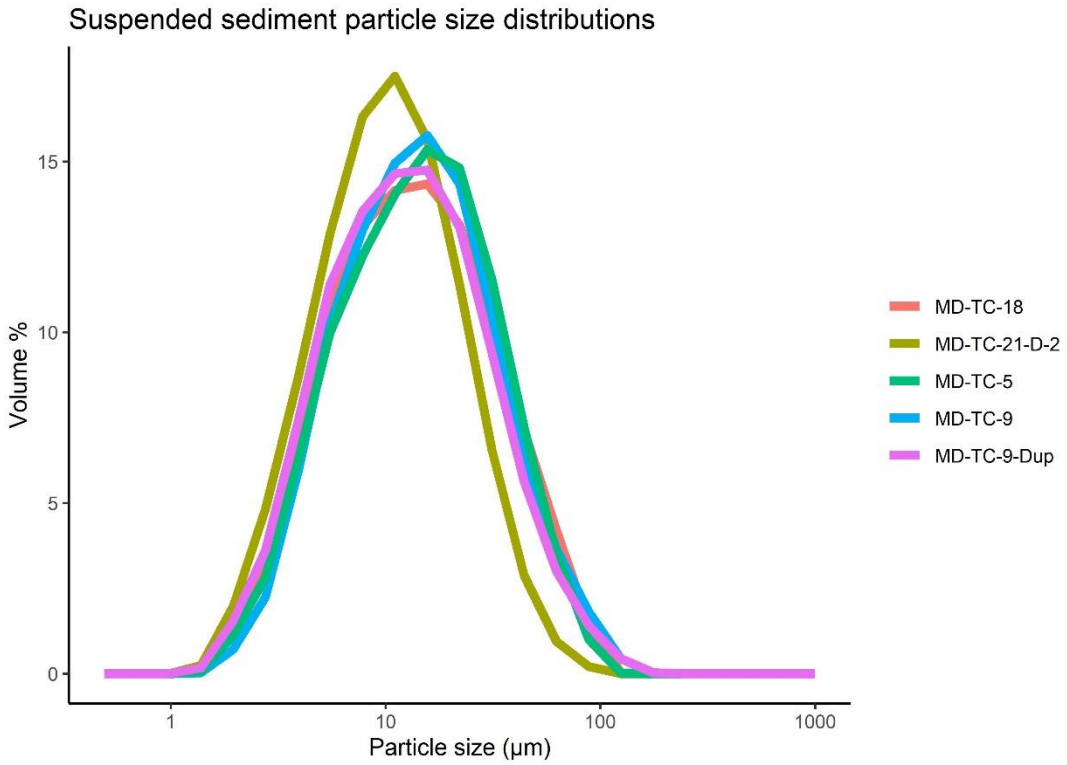

Figure 3: Approximate grain size distributions from suspended sediment samples along the sampled tidal channel transect, based on % volume of several aggregated grain size bins.

Dissolved organic carbon (DOC) (3.4 ± 0.6 mg/L) was relatively low (Supplementary Table 2). Most trace elements (i.e., V, Zn, Cr) are elevated well above average riverine dissolved element concentrations (Fig. B3), similar to other recent surface water studies in the area (Table B3). Dissolved Se and As are well above average river concentrations (0.07 µg/L and 0.62 µg/L, respectively) (Gaillardet et al., 2014). The mean concentration for As in the dissolved load was 57 ± 17 µg/L, while the mean concentration for Se was 39 ± 63 µg/L. Other elements of interest such as Ba (222 ± 71 µg/L), Co (1.0 ± 0.1 µg/L) and Ni (17 ± 4 µg/L) were significantly greater than average world river dissolved concentrations (23 µg/L, 0.148 µg/L, and 0.801 µg/L, respectively) (Gaillardet et al., 2014). Some elements (i.e., Be, Pb, Tl) analyzed had very low

concentrations close to or below detection limits, or negative values, and these elements were thus omitted from the reported results. Even though dissolved Cd values were quite low and sometimes below detection limit, none were negative, and were thus included for Kd calculations.

Suspended sediment element concentrations (Supplementary Table 3) are often less than or close to that of average upper continental crust (UCC) (Rudnick & Gao, 2003), although several trace elements are notably enriched relative to UCC such as Sb, Se, and Cd (Fig. 4A). Concentrations are generally greater than UCC for the most mobile elements during transport/weathering (right portion of Fig. 4A), while concentrations are less than UCC for the least mobile elements during transport/weathering (left portion of Fig. 4A). Suspended sediment barium concentrations are particularly low (72 ± 16 mg/kg; Supplementary Table 3). Element concentrations (particularly major elements) may be slightly less than if they were measured on an anhydrous basis. For comparisons to UCC, trace elements with measurements below detection limit were replaced with their detection limit values, rather than omitting the values below the MDL to prevent bias towards larger mean values. However, this may still slightly inflate the actual mean concentrations of several trace elements, such as Cd and Se. Several elements analyzed in the suspended sediment were routinely below detection limit and were thus omitted from the reported results (i.e., Be, Mo, Tl).

3.3 Partition coefficient values (Kd) between suspended and dissolved loads and the proportion in the dissolved load (D)

In this work, although suspended sediments represent multiple mineral phases, we use partition coefficients, known as Kd values, for simplicity to represent the bulk suspended sediment element concentration/total dissolved element concentration in L/kg in this study, which thus act as apparent Kd values (Table B2). While not equilibrium values, they provide a measure of element mobility. Most element Kd values decrease from left to right along the x-axis in Fig. 4B, although there are several exceptions. Mn and several trace elements like Co, Sb, As, Se, and Cd show higher Kd values than expected based on mobility trends (Fig. 4B). It is noted that trace elements such as As, Sb, Se, and Cd also have suspended sediment average element concentrations greater than UCC (Fig. 4A).

If the suspended sediment concentration (SSC; kg/L) is known, along with the Kd value of an element (L/kg), the dissolved proportion of that element can be calculated by:

$$D = \frac{1}{1+K_D*SSC} \quad (1)$$

Where D is the proportion of the element in the dissolved load based on mass within a theoretical 1L parcel of water that contains suspended sediment (Gaillardet et al., 2014). The proportion of the element in the suspended load is 1-D. As element mobility during transport and weathering increases from left to right along the x-axis, the proportion of the elements in the dissolved load also increases (Fig. 4C). Notable elements strongly deviating from the general trend are Co, Mn, Sb and Cd. For about half of the elements, transport in the dissolved load is dominant.

3.4 Element correlations/relationships

Major ions in solution (e.g., Mg, Ca, K, Cl, Na, SO_4) are strongly positively correlated with one another, while some trace elements (e.g., As and Se) tend to poorly correlate with other elements in the dissolved load (Fig. B4). However, Ni and Co are strongly positively correlated with most conservative ions in solution (Fig. B4).

Concentrations of many transition metals in the suspended sediment load display strong positive correlations (Fig. B5). In particular, trace metals are very well correlated with Fe and Al. Many metals (and P) show very strong trends of increasing concentration with increasing Fe content in the suspended sediment (Fig. B6). The metalloid As shows a moderate positive correlation with Fe in the suspended load.

3.5 Element trends with increased seawater mixing along the transect

A relatively consistent salinity trend can be seen with latitude (Fig. 2). As latitude decreases with increasing proximity to the Bay of Bengal, salinity increases, indicative of greater seawater mixing. This is also seen with strong negative associations between latitude and conservative ions in solution (Fig. B4).

As seawater mixing and thus salinity increases, Ni and Co concentrations increase in the dissolved load while their Kd values simultaneously decrease (Fig. 5). Arsenic and selenium display moderate to no relationship between Kd values and salinity along the transect (Fig. B7).

Elements in the suspended load predominantly show moderate to weak positive correlations with latitude and thus negative correlations with salinity (Fig. B5). For example, Ni and Co specifically show moderate negative correlations with salinity (Fig. B8) and thus moderate positive correlations with latitude (Fig. B5). These negative correlations with suspended load Ni and Co versus salinity are similar to trends seen with Ni and Co Kd values versus salinity and opposite the trends seen with Ni and Co dissolved concentrations (Fig. 5).

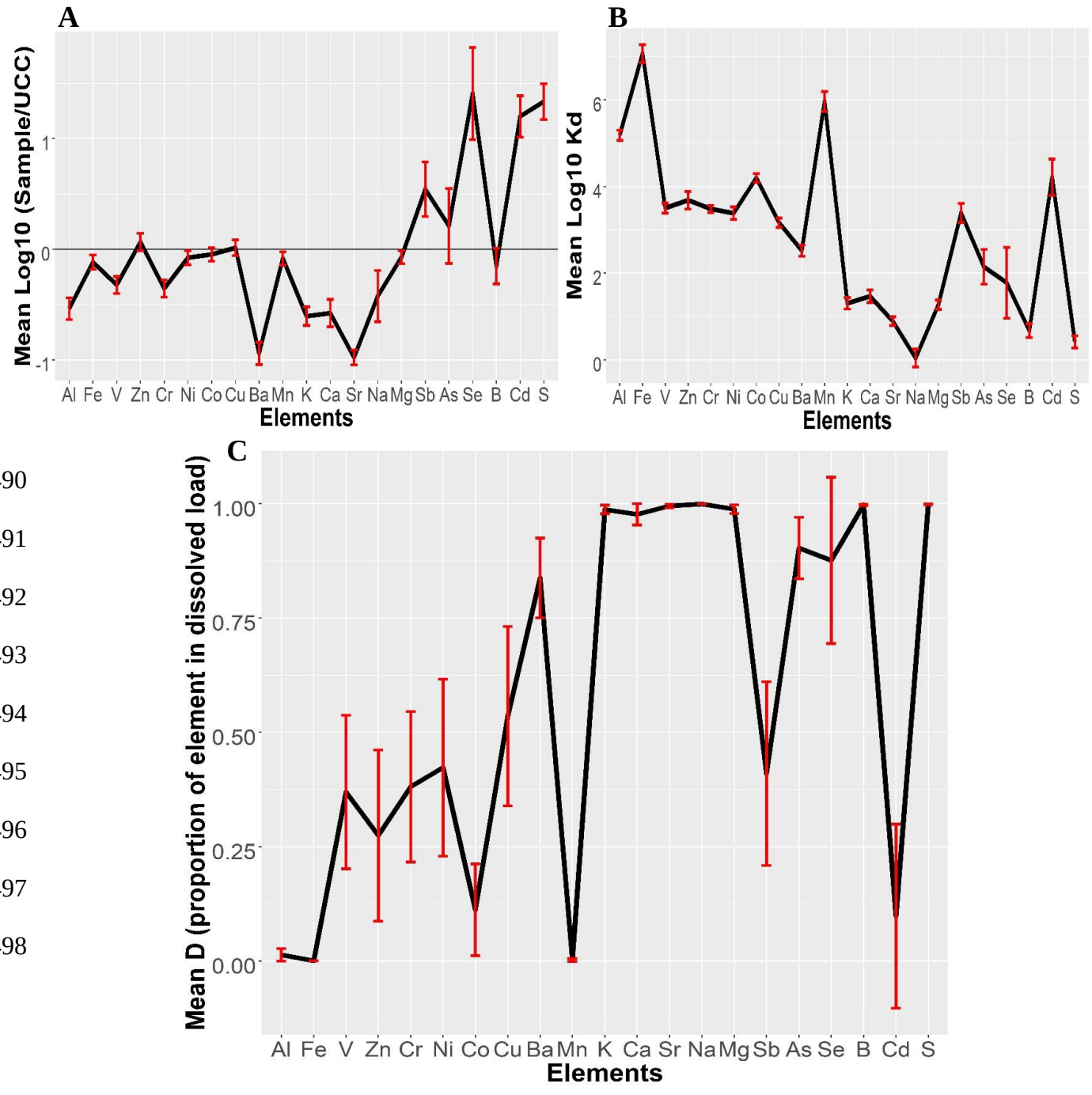

Figure 4: **(A)** Element concentrations in suspended sediment are normalized to upper continental crust (UCC) (Rudnick & Gao, 2003), with arithmetic mean log10 concentrations above 0 enriched relative to UCC and elements below 0 depleted relative to UCC. **(B)** Arithmetic mean log10 Kd values in L/kg (bulk concentration solid-phase/concentration dissolved-phase). **(C)** Estimated geometric mean proportion of each element in the dissolved load (D) within the upper 1m of the water column. The remaining proportion is the proportion of the element in the suspended load. For all graphs, the elements included are arranged to show increasing mobility during weathering and transport from left to right along the x-axis (Gaillardet et al., 2014). The red bars are 1 standard deviation (1 σ) error bars and MDLs are inserted for solid-phase concentrations <MDL to prevent bias towards greater concentrations. n = 21.

Barium shows unique trends in both the dissolved and suspended load as seawater mixing increases along the transect (Fig. 6). Dissolved Ba decreases as latitude decreases and seawater mixing increases, but not in a singular linear fashion. Instead, two different linear slopes of best fit are apparent along the transect. Additionally, Ba has a moderate positive correlation with its suspended sediment concentration and latitude, albeit there is significant scatter. Barium is strongly positively correlated with the extracted/measured Fe in the suspended load (Fig. 6). Barium Kd values are highest at lower latitudes close to the Bay of Bengal.

Both dissolved As and Se concentrations in the Bhairab River (that runs from the north of Khulna and meets the Rupsha River) are lower than values downstream of Khulna at lower

latitudes (Fig. 7 & Fig. B9). While As does not show gradually decreasing concentrations south of Khulna towards the Bay of Bengal (Fig. B9), Se does (Fig. 7).

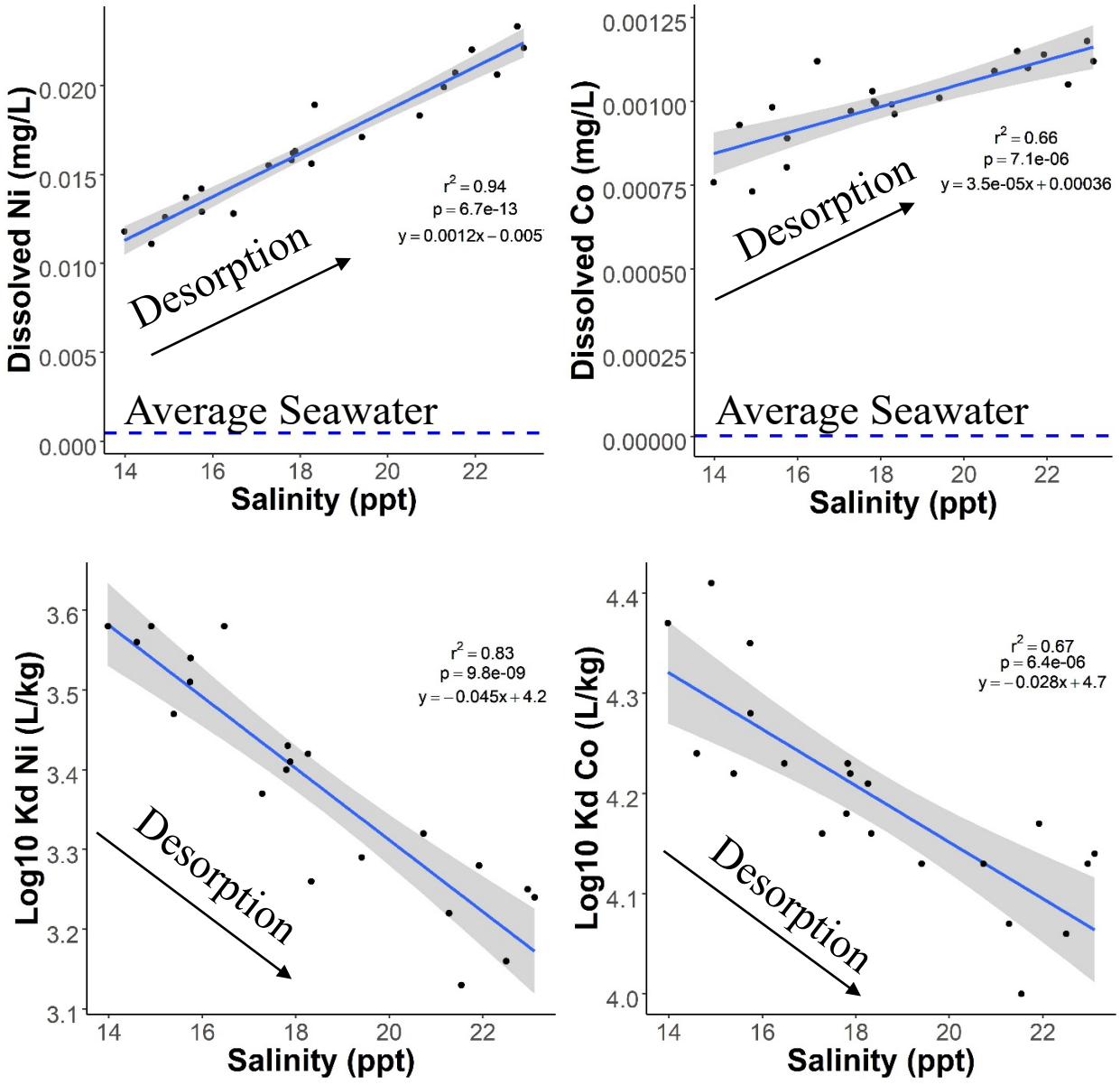

Figure 5: Salinity trends of Ni and Co Kd values (Log10 (L/kg)) with increased seawater mixing from higher to lower latitudes (upper row) and salinity trends of dissolved Co and Ni

values (mg/L) with increased seawater mixing from higher to lower latitudes – dashed blue lines represent average open ocean concentrations (lower row) (Mason, 2013). Shaded regions represent the 95% confidence interval about the linear regression line.

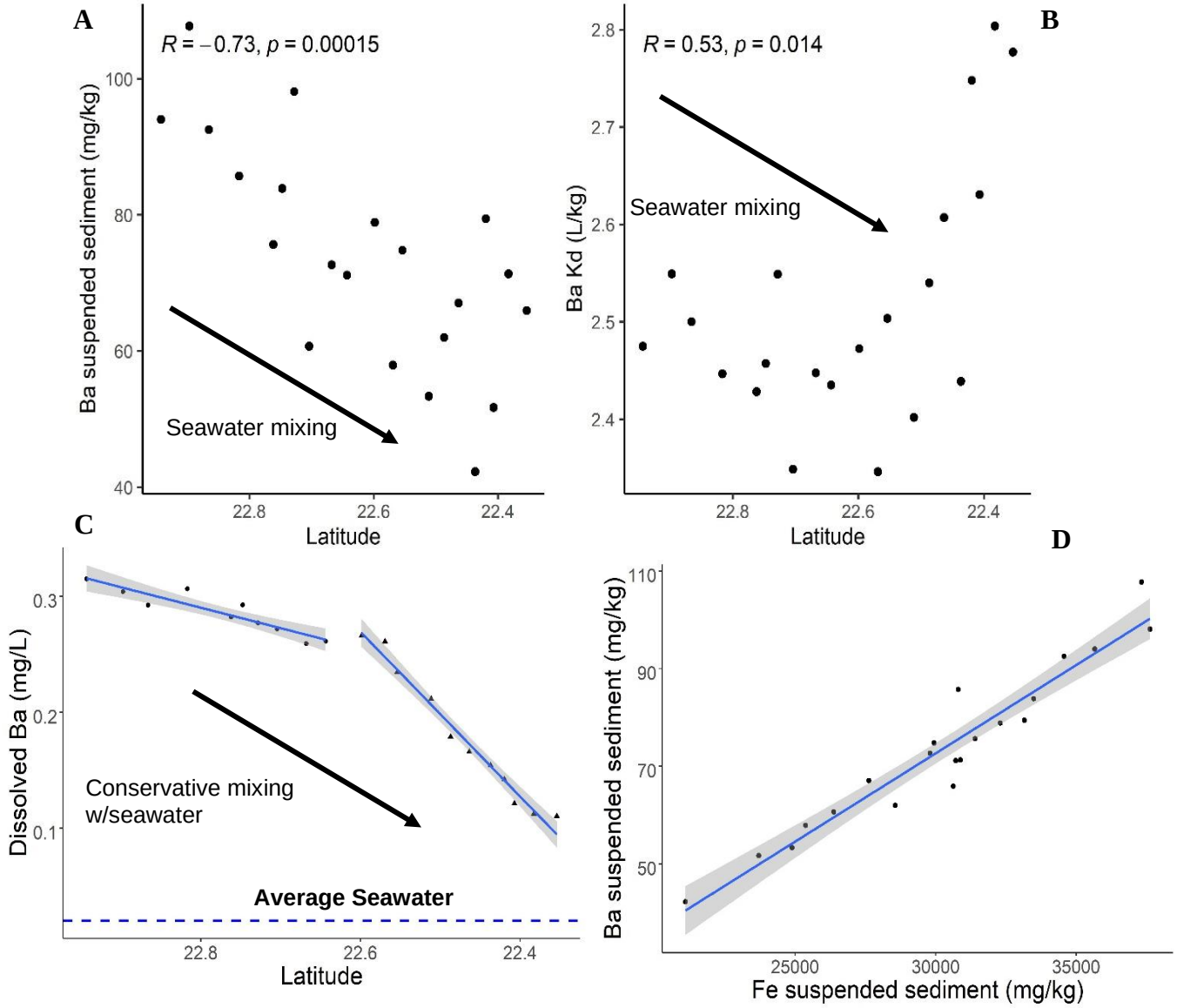

Figure 6: Various relationships of Ba with latitude and Fe, with (A) Ba concentration in the suspended load vs latitude, (B) Ba Kd values (L/kg) vs latitude, (C) Dissolved Ba vs latitude broken into two subpopulations with differing linear regression, and the blue dashed line

representing average seawater (Wright & Colling, 1995), (D) Suspended sediment Ba vs Fe concentrations in the suspended sediment load. Pearson correlation coefficient values are given with corresponding p-values in (A) and (B). Shaded regions are 95% confidence intervals about the linear regression lines in (C) and (D).

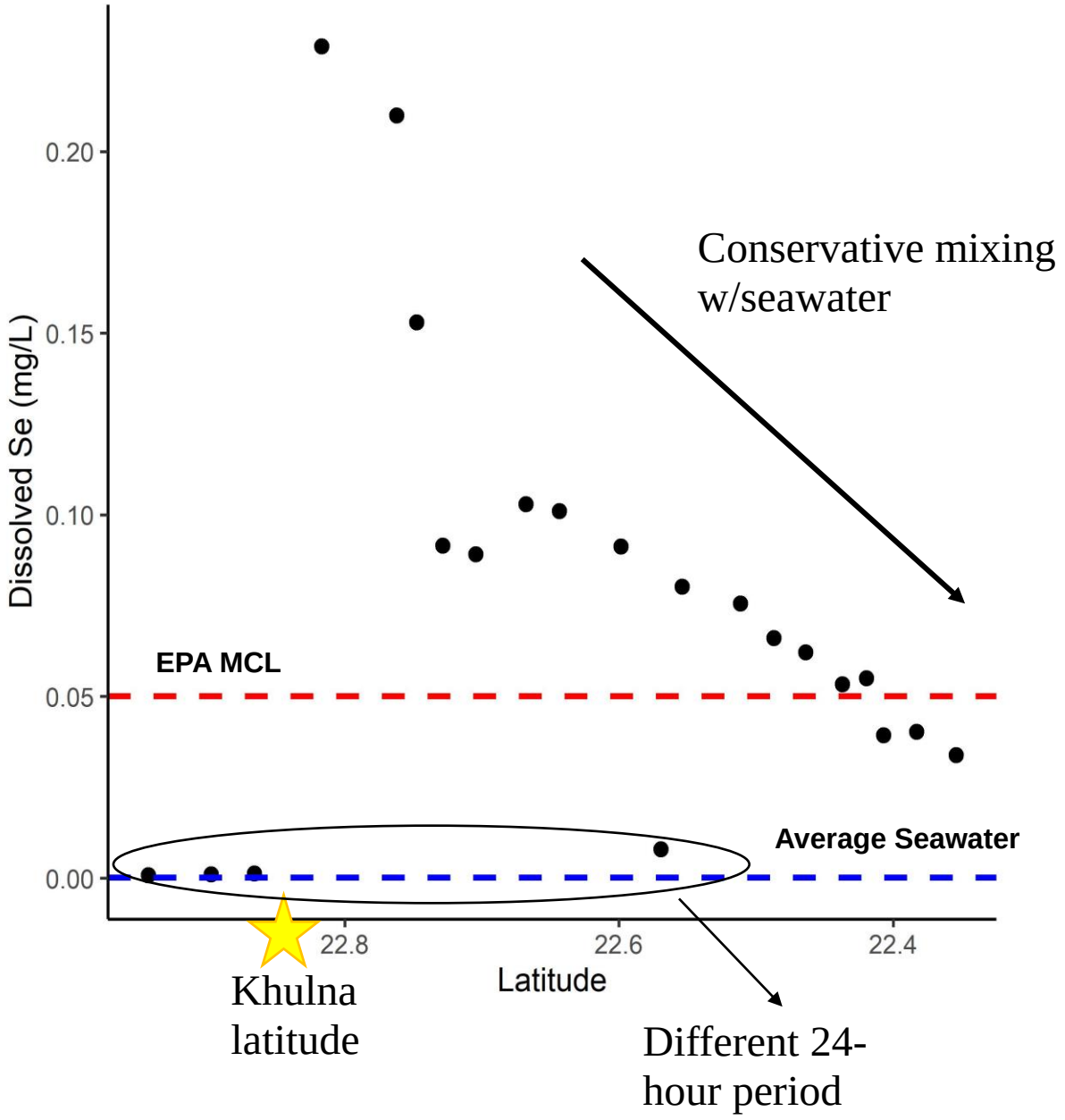

Figure 7: Dissolved selenium concentrations versus latitude, with the U.S. EPA drinking

water maximum contaminant level (MCL) represented by the red dashed line, average open ocean concentration (Mason, 2013) represented by the blue dashed line, the approximate latitude of Khulna marked with a star, and samples circled that were collected in a separate 24-hour period.

3.6 TEM particle imaging

TEM work on particulates from tidal channel suspended sediment within the study area and from this study routinely revealed small particles rich in Al and Si, likely to be clay minerals or other phyllosilicates (Figs. 8 & B14). Some of these particles had other elements such as Cu, Ti, and Fe associated with nanocrystals or coatings on their surfaces (mapped via STEM-EDS). A characteristic sample illustrates a striated surface containing several areas with higher concentrations of Fe and Cu, potentially attached to the larger particle surface as oxide nanoparticles (Fig. 8). Fe-rich particles <1μm were also common, including an Fe-particle near the filter size (0.2 μm) used in this study and several Fe-sulfide particles ~0.5 μm in diameter (Fig. B14). Several transition metals such as Mn, Ti, Ni, and Cu were found to be associated with these Fe-rich particles, although it is noted that the copper grid amplifies the Cu signal in EDS and elemental mapping, and the Ni EDS signal is weak (Fig. B14). Additionally, while mineralogical identification of the specific nanoparticles was difficult, a K-silicate particle with substantial K, Si and Al was identified that was likely a muscovite particle based on approximate wt.% and at.% proportions of Al, Si, O and K (Fig. B15).

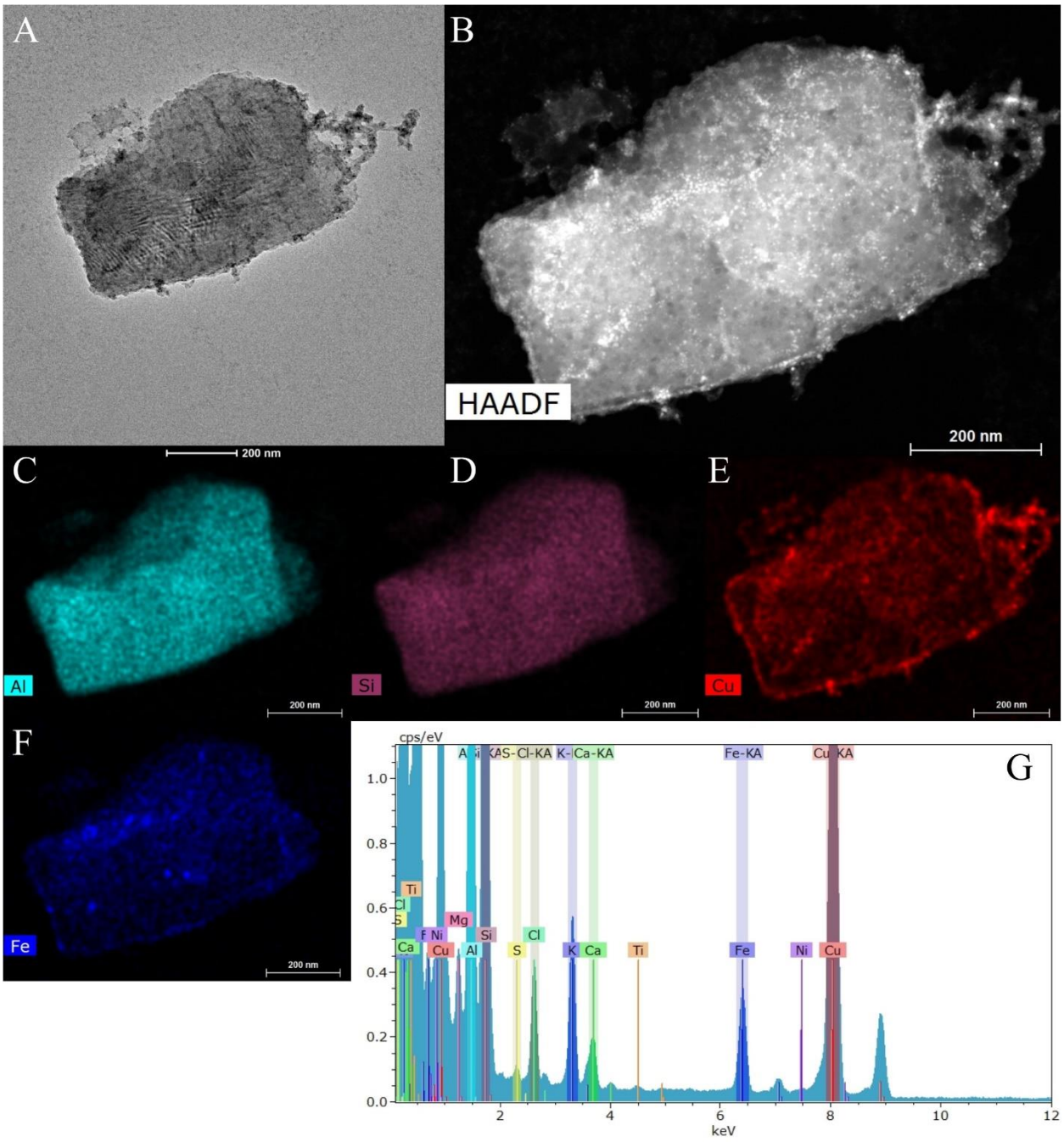

564

565 **Figure 8:** TEM analysis of a representative particulate from tidal channels in SW
566 Bangladesh (Sample P32-TC) (Dietrich & Ayers, 2021b). (A) TEM image shows a plate-like
567 particle with a striated surface about 1 μm in diameter. (B) High-angle annular dark-field
568 (HAADF) imagery illustrates the heavier atoms through brighter luminescence. STEM-EDS
569 maps are provided for the elements Al (C), Si (D), Cu (E), and Fe (F), which suggest an

aluminum-silicate particle with Cu and Fe-rich nanoparticles or ferric oxide coatings potentially on the surface. (G) The EDS spectrum of the sample with large peaks for each of the elements mapped, with Cu amplified because of the Cu TEM grid.

4 Discussion

4.1 Element enrichment/depletion in the dissolved and suspended loads

4.1.1 The dissolved load

Several trace elements (Ba, Ni, Co, Se, As) (Supplementary Table 2) normally seen in low concentrations in rivers' dissolved loads are elevated well above average world river dissolved load concentrations (Fig. B3). These element concentrations are similar to shrimp ponds and tidal channels from a previous study in the same region, which are also well above average seawater concentrations (Dietrich & Ayers, 2021b). However, relative to other recent studies of surface waters in the region, mean As and Cu concentrations were much greater in this study, while Cd, Fe, Mn, Pb, and Zn were much lower than the other studies (Table B3). These differences may be in part due to temporal sampling variability, spatial variability, or analytical procedures.

Arsenic and Se are well elevated above average dissolved riverine values (Gaillardet et al., 2014) in nearly all samples of this study, affirming that there must be a significant source

contributing these elements to the river system. Possible sources of As include geogenic sources such as leaching from sediments that contain As originally derived from the Himalayas, or groundwater due to exfiltration or irrigation (e.g., Ayers et al., 2017) because groundwater in the region contains elevated levels of As (e.g., Ayers et al., 2016). Arsenic can also be derived from anthropogenic sources, such as pesticides, herbicides, wood preservatives, and even animal feeds (Rosen & Liu, 2009). However, because of the prevalence of As-rich groundwater in the area, groundwater is deemed more likely as the ultimate source. This idea will be expanded upon in Section 4.2.3. While Se is less toxic than As and an essential micronutrient, it may still be harmful at elevated concentrations and may originate from fossil fuel burning (Rosen & Liu, 2009), municipal sewage or oil refinery effluent (Cutter & San Diego-McGlone, 1990), certain fertilizers (Girling, 1984), or the interaction of water with Se-rich rocks (Winkel et al., 2012). However, significant geogenic sourcing of Se thus far in Bangladesh has been shown to be limited, as soil concentrations are either typical of average world Se soil levels (Williams et al., 2009) or even lower (Spallholz et al., 2004), and groundwater Se concentrations have been well below health standards thus far and the concentrations of Se recorded in this study (e.g., Frisbie et al., 2002, 2009; Rahman et al., 2015). Possible anthropogenic sourcing of Se will also be discussed in more detail in Section 4.2.3.

While these tidal channels are not used for drinking water purposes during the dry season (i.e., early May) because of their high salinity, the elevated concentrations of dissolved Se and As may pose problems via accumulation in other biota. This is particularly because Southwest Bangladesh is an agricultural region that has been increasingly reliant upon shrimp aquaculture

615 in recent years (e.g., Khan et al., 2015) and uses tidal channels extensively for
616 agriculture/aquaculture irrigation (Ayers et al., 2017; Dietrich & Ayers, 2021b).
617
618 *4.1.2 The suspended load*
619
620 While most major elements (e.g., Al, Fe, K, Ca, Na) are depleted in the suspended
621 sediment load relative to upper continental crust (UCC), several trace elements (Se, As, Sb, Cd)
622 are enriched in most samples relative to UCC (Fig. 4A). Comparing elements in the suspended
623 load to a reference material such as UCC can give insight into regional enrichment or depletion
624 of solid-phase elements from transport, weathering or anthropogenic processes, assuming the
625 source material is similar in composition to the reference material (e.g., UCC). While the
626 composition of the source material in this study (eroded Himalayan crust) is difficult to constrain
627 with certainty (Lupker et al., 2012), average UCC can still provide a reasonable source
628 comparison, as various Himalayan formations that may contribute to the source material have
629 major element concentrations relatively similar to average UCC (A. Galy & France-Lanord,
630 2001). UCC has been commonly used in the region to evaluate anthropogenic influence on
631 sediments (e.g., Dietrich & Ayers, 2021a; Islam et al., 2017), and other factors that may
632 influence interpretation of anthropogenic enrichment (e.g., mineralogy and grain size) remain
633 relatively consistent in the upper 1m profile of river suspended sediment (e.g., Garzanti et al.,
634 2011).
635
636 The large depletion in Ca, Sr, Na, and K relative to UCC is likely representative of the
637 significant weathering of mobile elements that occurs in the Ganges floodplain prior to

deposition in the lower tidal plain (Bickle et al., 2018; Lupker et al., 2012), or grain size sorting effects. This depletion should hold true even if the major element concentrations in this study are slightly lower than they would be on an anhydrous basis like those used in UCC calculations (Rudnick & Gao, 2003). Previous work looking at deposited rice paddy and tidal channel sediment in Southwest Bangladesh also revealed depletion of mobile elements susceptible to weathering such as Sr, Na, and Ca, but saw enrichment of K relative to UCC (Ayers et al., 2020). The discrepancy between K concentrations between our study and Ayers et al. (2020) is perhaps partly attributable to grain size sorting, because the volume-weighted mean grain size of the deposited sediments were oftentimes 2-3 times greater than the grain size of suspended sediment samples in this study. This is reflective of the upper portion of the water column (i.e., upper 1m used in this study) containing the finest grained sediment compared to the rest of the water column (e.g., Garzanti et al., 2011). The coarser material in Ayers et al. (2020) may have greater abundances of K-rich minerals, such as K-feldspar, which was observed in suspended sediment profiles in the Ganges and Brahmaputra rivers as grain size increases with depth (Garzanti et al., 2011). However, mineralogical data in this study for both suspended sediment and shrimp pond sediment (Fig. B2) is remarkably similar to the sediment in Ayers et al. (2020) based on qualitative observations of diffraction peaks, suggesting that grain size sorting within the silt sized range may not have a large effect on mineral abundance. This similar mineralogy is also consistent with the shrimp pond sediment being sourced from the tidal channel. Additionally, TEM analyses identified a K-silicate particle that is likely muscovite in our suspended sediment (Fig. B15), illustrating at least one of the K-phases present in sediment.

The enrichment of several trace elements such as Se, Cd, As and Sb and dissimilarities to the comparatively lower concentrations of several trace elements such as Sb, Cd and As in Ayers et al. (2020) could be partly due to the finer grain size of the suspended sediments in the upper 1m of the water column. The smaller grain sizes (with presumably larger surface area) may be more effective at scavenging elements like Cd and As than the slightly coarser grains in Ayers et al. (2020). The elevated trace element concentrations may also be in part due to anthropogenic inputs (e.g., Garzanti et al., 2011), such as from the city of Khulna, or because of volatilization of several trace elements during the $LiBO_2$ flux fusion procedures in Ayers et al. (2020) leading to trace element depletion in that study. Enrichment of trace elements such as As, Se, Cd, and Sb relative to UCC was also reported in suspended sediment in the upper Ganges (Boral et al., 2020), suggesting that the geogenic contribution of these trace elements from sediments in the Ganges river system may be greater than typical crustal values.

4.2 Geochemical trends with increased seawater mixing

4.2.1 Evidence of trace metal desorption along the transect

As latitude decreases along the tidal channel transect and the sample locations approach the Bay of Bengal, salinity increases (Fig. 2). Thus, any spatial trends associated with latitude can also be interpreted as trends with salinity. The trace metals Ni and Co typically exhibit nonconservative behavior and have dissolved concentrations that are well above seawater (Mason, 2013) and increase linearly as salinity increases (Fig. 5). Thus, the increasing dissolved concentrations of these metals with increased seawater mixing cannot be explained by simple

683 conservative mixing of seawater. A source other than seawater must be responsible for the
684 increasing concentration of these trace metals.
685
686 One likely source of dissolved Ni and Co is suspended sediment, as desorption of Co and
687 Ni from suspended sediment has been documented in a nearby estuary (Hooghly Estuary, ~100-
688 150 km to the west of the study area) with increased seawater mixing (Samanta & Dalai, 2018).
689 That study saw the same linear trends of increasing dissolved Co and Ni with increasing salinity
690 (Samanta & Dalai, 2018). Furthermore, that study showed Kd values decreasing with salinity,
691 suggestive of desorption from competitive cation interactions, which is consistent with the Kd
692 trends of Ni and Co in our study (Fig. 5). Our lower suspended sediment concentrations of Ni
693 and Co at higher salinities also supports some level of desorption occurring (Fig. B8). While the
694 Kd values from Samanta & Dalai (2018) were based on the exchangeable solid fractions of Ni
695 and Co, the bulk (apparent) Kd values used in this study can still provide a similar approximation
696 of partitioning. This is because a main objective of our study was to characterize changes of
697 element concentrations in the suspended/dissolved load with increased seawater mixing, and
698 apparent Kd values are still an ample way to quantify that, especially as most of our sediments
699 consisted of similar grain size and silty-clay composition and thus likely similar exchangeable
700 fractions of elements.
701
702 However, Samanta & Dalai (2018) also showed Cu exhibiting similar characteristics to
703 Ni and Co with increased seawater mixing, which our study did not observe (Fig. B16).
704 Additionally, Samanta & Dalai (2018) attributed the desorption processes largely to competition
705 with Na for sorption sites, which we did not see direct evidence of based on our Na

concentrations. This may be because Samanta & Dalai (2018) utilized data from suspended sediment that was rinsed with Milli-Q water, which may have removed some Na, Mg, and K from sea salt that was likely included in our suspended sediment analysis (the lack of rinsing salts from our suspended sediment samples may also be the reason S is elevated relative to UCC (Fig. 4A), because of soluble sulfate minerals precipitating from seawater after drying).

4.2.2 Barium trends along the transect

Dissolved Ba in general exhibits decreasing concentration as salinity increases (Fig. 6C). This is indicative of conservative mixing with seawater, which is seen in other studies in the region at salinities equivalent to this study (>10 ppt) (Carroll et al., 1993; Moore, 1997; Samanta & Dalai, 2016). However, a distinct change in linear regression slope is observed at a latitude of ~22.6 in this study (Fig. 6C), also when the transect transitions from the Rupsha River to the Bhadra River. This may indicate a decrease of Ba supplied to the dissolved load from sediment desorption (and thus increasing the rate/slope of conservative mixing), as both Ba Kd values and suspended sediment concentrations either remain stable or increase at lower latitudes (Figs. 6A & 6B). Other studies of Ba in the region indicate dissolved Ba increasing at low salinities due to sediment desorption from cation substitution (Carroll et al., 1993; Moore, 1997; Samanta & Dalai, 2016), which would explain the Ba concentrations in this study being well above average riverine Ba concentrations (Gaillardet et al., 2014) if Ba desorption occurred upstream of our study area. Barium is strongly correlated with Fe in the sediment load as well (Fig. 6D), suggesting that the fraction of solid-phase Ba analyzed in this study is associated with Fe-

minerals such as Fe-oxyhydroxides, which a large portion of labile Ba is associated with (e.g., Carter et al., 2020).

Barium may also be introduced into tidal channels from groundwater exfiltration, particularly because average Ba (380 µg/L; Ayers et al., 2016) is elevated in groundwaters in the area relative to tidal channel samples in this study (~220 µg/L) and Ganges-Brahmaputra river representative values (~21 µg/L; Dowling et al., 2003). Moore (1997) and Dowling et al. (2003) assert that a large flux of the dissolved Ba in the Bay of Bengal is indeed from groundwater discharge. However, because desorption of Ba from tidal channel sediment or upstream river sediment is likely contributing substantial dissolved Ba (e.g., Carroll et al., 1993) and the proportion of groundwater exfiltration to tidal channels is probably less than to the Bay of Bengal, groundwater Ba contribution to tidal channels is likely less than that of sediment desorption upstream.

4.2.3 Arsenic and selenium trends along the transect

Arsenic and selenium have been previously documented in concentrations above drinking water guidelines in Southwest Bangladesh surface waters (Ayers et al., 2017; Dietrich & Ayers, 2021b), and thus this study set out to investigate whether the large city of Khulna could possibly be a source of these elements downstream. Previous work found several potential "hotspots" of Zn and U pollution in waterways near our study area through artificial mussel monitoring, albeit pollution was less in Khulna waterways compared to the Buriganga River in Dhaka (Kibria et al.,

2016). However, that study did not analyze for Se or As, and As and Se were elevated well above typical riverine values in this study (Supplementary Table 2).

Both selenium and arsenic exhibit the lowest concentrations in the Bhairab River along the more northern extent of Khulna at the highest latitudes in this study (Fig. 7 and Fig. B9). However, while As did not display any definitive mixing trends downstream (Fig. B9), Se showed conservative mixing with decreasing latitude and increased salinity for all samples but the three Bhairab River samples and another sample downstream (which was taken within a separate 24-hour sampling period at a similar time of day as previous nearby samples, and during the same 24-hour sampling period as the three Bhairab River samples) (Fig. 7). Conservative mixing of dissolved Se with seawater has been documented before, specifically when it was anthropogenically sourced to San Francisco Bay in the U.S. (Cutter, 1989). However, the dissolved Se concentrations in this study are much higher than in polluted estuary samples of other studies and are much closer to direct oil refinery effluent Se concentrations (Cutter, 1989; Cutter & San Diego-McGlone, 1990). Khulna holds two large petroleum companies along the southern reaches of the Bhairab, which are a possible source of the downstream Se. However, based on watersheds of both the Bhairab and Rupsha rivers (Fig. B17), it is possible that Se may have been sourced upstream of Khulna. Selenium has no known geogenic sources of such high concentrations in the area, as soils (Spallholz et al., 2004; Williams et al., 2009) and groundwater (Frisbie et al., 2002, 2009; Rahman et al., 2015) are not anomalously high in Se in Bangladesh. Thus, Se is likely anthropogenic. Our interpretations of anthropogenic Se support recent work in the Ganges river system in India, where trace element pollutant hotspots have been identified near cities, but typically do not persist downstream because of dilution from additional river

773 tributaries (Boral et al., 2020). In our case, the dilution is caused by seawater mixing in lieu of
774 other river tributaries.
775
776 Because dissolved As is relatively ubiquitously elevated in samples irrespective of
777 latitude with no definitive trends (Fig. B9), a possible source may be from groundwater during
778 dry season low river flow, as previously suggested by Ayers et al. (2017). However, assuming
779 groundwater contribution was consistent along the transect, it would be expected that there
780 would be conservative mixing of arsenic as the seawater fraction increases along the transect,
781 unless some of the reworked tidal channel water from the Bay of Bengal contains As from
782 submarine discharge. However, it is unlikely that the water from the Bay of Bengal would
783 contain elevated As. Thus, either As is not sourced predominantly from groundwater or
784 additional nonconservative processes are at work regarding As mobilization and transport,
785 perhaps because of interactions of groundwater at redox zones between the sediment-water
786 interface such as proposed by Berube et al. (2018). Arsenic from reducing groundwaters may
787 sorb onto sediments in oxidizing environments before discharging into rivers, although if
788 riverine dissolved As is sourced from groundwater, there must be exfiltration points where
789 sorption is limited and redox conditions are thus not suitable for complete As sorption. Thus,
790 variability in these redox transition zones of groundwater exfiltration may partially explain the
791 nonconservative mixing seen between As and seawater (Fig. B9), or alternatively, there is
792 colloidal transport of As into tidal channels with these redox transition zones as the source.
793
794 Samples with high concentrations of dissolved selenium that fall on a conservative
795 mixing trend may specifically be sourced from an anthropogenic effluent flushing event (Fig. 7).

The four samples with the lowest concentrations were taken in a different 24-hour period (Fig. 7). However, the relatively ubiquitously elevated Se concentrations in July shrimp ponds and May shrimp ponds in Southwest Bangladesh relative to average riverine concentrations (Dietrich & Ayers, 2021b) suggests that if the Se is ultimately sourced from effluent discharge, it is not from isolated events. Lastly, it is important to note that Se was an order of magnitude lower (1 µg/L vs 30 µg/L) in a sample of the Bhairab River in this study compared to Dietrich & Ayers (2021b) (Fig. B11), who field filtered at 0.45 µm at the same location. One likely cause of the discrepancy between samples is the filtration size difference [0.2 µm in this study versus 0.45 µm in Dietrich & Ayers (2021b)], where small, colloidal-like particles (organic or inorganic) may increase filtered "dissolved" concentrations (Gaillardet et al., 2014). This may impact the transition metals Cr, Cu, Zn, Co, and Ni, as well as Se and P in this study where inconstancies between lab and field-filtered samples were observed, particularly because of evidence of colloidal particles containing Fe-rich coatings with traces of Mn, Ni, and Cu (Figs. 8 and B14).

Both As and Se Kd values do not show any obvious trends with salinity (and therefore seawater mixing) along the transect (Fig. B7). This suggests that these elements are not strongly influenced by sorption or dissolution reactions along the transect as salinity increases. However, analysis of the extractable fractions of each element (at lower instrument detection limits) will provide better insight into possible element exchange, particularly for As, which is likely experiencing nonconservative processes based on the lack of conservative mixing seen along the transect (Fig. B9).

4.3 Possible sample incubation effects

819

820 Because several effects may occur during long incubation times of unfiltered water
821 samples (i.e., dissolution, sorption reactions, biological reactions), the effect of incubation time
822 on several geochemical parameters of interest was examined. Most dissolved and solid phase
823 elements and geochemical parameters were not strongly correlated with days between sampling
824 and lab filtration (Figs. B4 & B5). Importantly, most tidal channel waters are reworked within
825 the system (Hale et al., 2019), leading to residence times of water and suspended sediment within
826 the relative magnitude of our sample incubation time. More detailed discussion is provided as
827 Supporting Information (Text B2), but it is interpreted that the effects of sample storage were not
828 significant enough to affect the main geochemical interpretations of this work.

829

830 *4.4 Summary of geochemical mechanisms*

831

832 The primary mechanisms hypothesized to affect the distribution and partitioning of
833 elements along this study's transect were desorption, ion-exchange, and conservative mixing
834 with seawater. Changes in pH and dissolution might also be expected to influence element
835 partitioning in an estuarine environment, although direct evidence of these mechanisms causing
836 changes along the transect is lacking. pH measurements showed very little variation along the
837 transect ($1\sigma = 0.09$; Supplementary Table 1), and although the pH values were lower than one
838 might expect based on mixing with seawater, the lack of variation indicates that pH has little
839 effect on changing element concentrations throughout the transect. However, the slightly alkaline
840 pH (mean = 7.61) likely leads to preference for cation adsorption on HFOs as opposed to anion
841 species such as arsenate, selenate, or selenite, because the points of zero charge and isoelectric

842 points are estimated as between ~7-8.5 for HFOs (Kosmulski, 2018). While dissolution can play
843 an important role in element partitioning in coastal environments, it is difficult to deduce the
844 extent it occurs in the natural environment, particularly in this study because of difficulty
845 distinguishing dissolution processes in highly saline waters (e.g., Jeandel & Oelkers, 2015).
846 However, minerals that are major components of river sediments in Bangladesh and are present
847 in suspended sediment such as quartz, kaolinite and illite (e.g., Datta & Subramanian, 1997; Fig.
848 B2) have low laboratory dissolution rates (e.g., Jeandel & Oelkers, 2015) and are saturated in our
849 water samples (Supplementary Table 1), suggesting that dissolution of suspended sediments
850 during transport was low in our study area. Furthermore, annual dissolution in seawater is
851 estimated to be close to 0% for those minerals (e.g., Jeandel & Oelkers, 2015). Lastly, Ayers et
852 al. (2020) classifies sediment weathering in this study region as likely transport limited, which
853 our measurements of depleted Na, Ca, and K support (Fig. 4A), and thus dissolution reactions
854 are slow if they are occurring.
855
856 Because of the focus of this study on trace elements rather than major elements, it is
857 unclear to what extent major elements exchanged with one another on solid surface sites via ion
858 exchange. However, there is evidence of saltwater major cation substitution leading to desorption
859 of Ni and Co along the transect of this study with increased mixing of seawater. This may have
860 significant impacts on dissolved estuarine fluxes into the ocean, particularly if there is an
861 upstream pollution spill of Ni or Co, or a similar metal cation species. While these cations may
862 adsorb effectively onto suspended sediment in lower salinity water, they may be mobilized in
863 higher salinity water, which could pose a threat for biota in ecosystems such as the Sundarbans,
864 or for farmers who irrigate with the saline tidal channel water for aquaculture. Lastly, while

conservative mixing of elements such as saltwater ions may be obvious with increased seawater contribution, conservative mixing of other elements such as Ba and Se following a nonconservative input source (desorption or effluent release) provides more insight into the dilution and behavior of these elements in estuarine environments. Thus, all hypothesized geochemical mechanisms affect element partitioning to some degree, but elements are affected in different ways. Better understanding of which elements are likely associated with certain processes can be useful for research in other estuary environments throughout the world, such as the Mississippi River delta or Red River delta.

5 Conclusions

Multiple processes affect element mobility and transport along tidal channels in Bangladesh, such as desorption, ion-exchange, and conservative mixing. The elements Ni and Co are affected by desorption processes induced by exchange with saltwater cations. Barium shows trends consistent with conservative mixing with seawater, although it too is likely affected by desorption processes, albeit largely upstream in lower salinity waters. Selenium is elevated well above typical riverine dissolved concentrations and is likely anthropogenically sourced from the city of Khulna or another site farther upstream. Arsenic is also well above average riverine dissolved concentrations and is likely predominantly geogenic and may be partly sourced from groundwater exfiltration, like Ba.

Most trace elements are elevated above average dissolved river concentrations, and further monitoring of anthropogenic pollution sources upstream is needed to protect the Sundarbans natural mangrove forest. If there is any significant release of metal cations upstream

such as Ni and Co, they may be increasingly mobilized in the saline, estuarine environment of the Sundarbans' tidal channels, particularly during the dry season.

Collectively, geochemical measurements along a tidal channel transect in Southwest Bangladesh illustrate the complex estuarine processes at work, affecting trace elements in dynamic ways. These processes are likely also occurring to various degrees in other coastal estuarine systems that experience seasonality and tidal influence. Thus, it is essential to perform detailed geochemical measurements of the dissolved and suspended loads in coastal estuaries throughout the world to better understand the impacts estuaries have on elemental fluxes and cycling, particular in the context of increased climate and anthropogenic change in coming years.

Conflict of interest

There are no conflicts of interest to declare.

Acknowledgements

Funding supported by the NSF Coastal SEES Collaborative Research Grant OCE-1600319. We appreciate the thoughtful comments from Jessica Oster during earlier drafts of the manuscript. We thank the editorial handling of the associate editor and detailed comments from an anonymous reviewer that greatly strengthened the quality of the manuscript. Special thanks to Md. Zahidul Haque for his immense help in the field and to many others from the University of Dhaka, Khulna University and Pugmark Tours (Md Nazrul Islam (Bachchu)) who have helped with this ongoing research project. Thanks also goes out to Rossane DeLapp, James McBride and the Vanderbilt Institute of Nanoscale Science and Engineering (VINSE), Christopher Sharp,

and Sunjeong Park and the Ohio State University Service Testing and Research Laboratory (STAR Lab) for analytical assistance.

References

Ahmed, K., Mehedi, Y., Haque, R., & Mondol, P. (2011). Heavy metal concentrations in some macrobenthic fauna of the Sundarbans mangrove forest, south west coast of Bangladesh. *Environmental Monitoring and Assessment*, *177*(1), 505–514. https://doi.org/10.1007/s10661-010-1651-9

Akai, J., Izumi, K., Fukuhara, H., Masuda, H., Nakano, S., Yoshimura, T., Ohfuji, H., Md Anawar, H., & Akai, K. (2004). Mineralogical and geomicrobiological investigations on groundwater arsenic enrichment in Bangladesh. *Applied Geochemistry*, *19*(2), 215–230. https://doi.org/10.1016/j.apgeochem.2003.09.008

Akter, S., & Ahmed, K. R. (2019). Water chemistry and water quality of a tidal river system in relation with riverbank land use pattern and regional climate in the southwest Bengal Delta of Bangladesh. *Sustainable Water Resources Management*, *5*(3), 1259–1279. https://doi.org/10.1007/s40899-019-00308-3

Anawar, H. M., Akai, J., Komaki, K., Terao, H., Yoshioka, T., Ishizuka, T., Safiullah, S., & Kato, K. (2003). Geochemical occurrence of arsenic in groundwater of Bangladesh: Sources and mobilization processes. *Journal of Geochemical Exploration*, *77*(2), 109–131. https://doi.org/10.1016/S0375-6742(02)00273-X

Ayers, J. C., George, G., Fry, D., Benneyworth, L., Wilson, C., Auerbach, L., Roy, K., Karim, Md. R., Akter, F., & Goodbred, S. (2017). Salinization and arsenic contamination of

surface water in southwest Bangladesh. *Geochemical Transactions*, *18*(1), 4. https://doi.org/10.1186/s12932-017-0042-3

Ayers, J. C., Goodbred, S., George, G., Fry, D., Benneyworth, L., Hornberger, G., Roy, K., Karim, Md. R., & Akter, F. (2016). Sources of salinity and arsenic in groundwater in southwest Bangladesh. *Geochemical Transactions*, *17*(1), 4. https://doi.org/10.1186/s12932-016-0036-6

Ayers, J. C., Patton, B., & Dietrich, M. (2020). Preliminary Evidence of Transport-Limited Chemical Weathering and Element Immobility in the Ganges Tidal Delta Plain of Bangladesh. *Geochemistry, Geophysics, Geosystems*, *21*(8), e2020GC009029. https://doi.org/10.1029/2020GC009029

Berube, M., Jewell, K., Myers, K. D., Knappett, P. S. K., Shuai, P., Hossain, A., Lipsi, M., Hossain, S., Hossain, A., Aitkenhead-Peterson, J., Ahmed, K. M., Datta, S., Berube, M., Jewell, K., Myers, K. D., Knappett, P. S. K., Shuai, P., Hossain, A., Lipsi, M., … Datta, S. (2018). The fate of arsenic in groundwater discharged to the Meghna River, Bangladesh. *Environmental Chemistry*, *15*(2), 29–45. https://doi.org/10.1071/EN17104

Bethke, C. M. (2007). *Geochemical and Biogeochemical Reaction Modeling*. Cambridge University Press.

Bickle, M. J., Chapman, H. J., Tipper, E., Galy, A., De La Rocha, C. L., & Ahmad, T. (2018). Chemical weathering outputs from the flood plain of the Ganga. *Geochimica et Cosmochimica Acta*, *225*, 146–175. https://doi.org/10.1016/j.gca.2018.01.003

Boral, S., Sen, I. S., Tripathi, A., Sharma, B., & Dhar, S. (2020). Tracking Dissolved Trace and Heavy Metals in the Ganga River From Source to Sink: A Baseline to Judge Future

Changes. *Geochemistry, Geophysics, Geosystems*, *21*(10), e2020GC009203. https://doi.org/10.1029/2020GC009203

Brammer, H. (2014). Bangladesh's dynamic coastal regions and sea-level rise. *Climate Risk Management*, *1*, 51–62. https://doi.org/10.1016/j.crm.2013.10.001

Carroll, J., Falkner, kelly K., Brown, E. T., & Moore, W. S. (1993). The role of the Ganges-Brahmaputra mixing zone in supplying barium and226Ra to the Bay of Bengal. *Geochimica et Cosmochimica Acta*, *57*(13), 2981–2990. https://doi.org/10.1016/0016-7037(93)90287-7

Carter, S. C., Paytan, A., & Griffith, E. M. (2020). Toward an Improved Understanding of the Marine Barium Cycle and the Application of Marine Barite as a Paleoproductivity Proxy. *Minerals*, *10*(5), 421. https://doi.org/10.3390/min10050421

Chowdhury, N. T. (2010). Water management in Bangladesh: An analytical review. *Water Policy*, *12*(1), 32–51. http://dx.doi.org/10.2166/wp.2009.112

Cutter, G. A. (1989). The estuarine behaviour of selenium in San Francisco Bay. *Estuarine, Coastal and Shelf Science*, *28*(1), 13–34. https://doi.org/10.1016/0272-7714(89)90038-3

Cutter, G. A., & San Diego-McGlone, M. L. C. (1990). Temporal variability of selenium fluxes in San Francisco Bay. *Science of The Total Environment*, *97–98*, 235–250. https://doi.org/10.1016/0048-9697(90)90243-N

Datta, D. K., Ghosh, P. K., Karim, Md. R., & Rahman, Md. M. (2020). Geochemical options for water security in a coastal urban agglomerate of Lower Bengal Delta, Bangladesh. *Journal of Geochemical Exploration*, *209*, 106440. https://doi.org/10.1016/j.gexplo.2019.106440

978 Datta, D. K., & Subramanian, V. (1997). Texture and mineralogy of sediments from the Ganges-
979 Brahmaputra-Meghna river system in the Bengal Basin, Bangladesh and their
980 environmental implications. *Environmental Geology*, *30*(3–4), 181–188.
981 https://doi.org/10.1007/s002540050145
982 de Souza Machado, A. A., Spencer, K., Kloas, W., Toffolon, M., & Zarfl, C. (2016). Metal fate
983 and effects in estuaries: A review and conceptual model for better understanding of
984 toxicity. *Science of The Total Environment*, *541*, 268–281.
985 https://doi.org/10.1016/j.scitotenv.2015.09.045
986 Dietrich, M., & Ayers, J. (2021a). Geochemical partitioning and possible heavy metal(loid)
987 bioaccumulation within aquaculture shrimp ponds. *Science of The Total Environment*,
988 *788*, 147777. https://doi.org/10.1016/j.scitotenv.2021.147777
989 Dietrich, M., & Ayers, J. C. (2021b). Influences on tidal channel and aquaculture shrimp pond
990 water chemical composition in Southwest Bangladesh. *Geochemical Transactions*, *22*(1),
991 2. https://doi.org/10.1186/s12932-021-00074-2
992 Dowling, C. B., Poreda, R. J., & Basu, A. R. (2003). The groundwater geochemistry of the
993 Bengal Basin: Weathering, chemsorption, and trace metal flux to the oceans. *Geochimica*
994 *et Cosmochimica Acta*, *67*(12), 2117–2136. https://doi.org/10.1016/S0016-
995 7037(02)01306-6
996 Fendorf, S., Michael, H. A., & van Geen, A. (2010). Spatial and Temporal Variations of
997 Groundwater Arsenic in South and Southeast Asia. *Science*, *328*, 5.
998 Frisbie, S. H., Mitchell, E. J., Mastera, L. J., Maynard, D. M., Yusuf, A. Z., Siddiq, M. Y.,
999 Ortega, R., Dunn, R. K., Westerman, D. S., Bacquart, T., & Sarkar, B. (2009). Public
1000 Health Strategies for Western Bangladesh That Address Arsenic, Manganese, Uranium,

and Other Toxic Elements in Drinking Water. *Environmental Health Perspectives*, *117*(3), 410–416. https://doi.org/10.1289/ehp.11886

Frisbie, S. H., Ortega, R., Maynard, D. M., & Sarkar, B. (2002). The concentrations of arsenic and other toxic elements in Bangladesh's drinking water. *Environmental Health Perspectives*, *110*(11), 1147–1153. https://doi.org/10.1289/ehp.021101147

Gaillardet, J., Dupré, B., Louvat, P., & Allègre, C. J. (1999). Global silicate weathering and CO2 consumption rates deduced from the chemistry of large rivers. *Chemical Geology*, *159*(1), 3–30. https://doi.org/10.1016/S0009-2541(99)00031-5

Gaillardet, J., Viers, J., & Dupré, B. (2014). Trace Elements in River Waters. In H. D. Holland & K. K. Turekian (Eds.), *Treatise on Geochemistry* (pp. 225–272). Pergamon. https://doi.org/10.1016/B0-08-043751-6/05165-3

Galy, A., & France-Lanord, C. (2001). Higher erosion rates in the Himalaya: Geochemical constraints on riverine fluxes. *Geology*, *29*(1), 23–26. https://doi.org/10.1130/0091-7613(2001)029<0023:HERITH>2.0.CO;2

Galy, V., France-Lanord, C., & Lartiges, B. (2008). Loading and fate of particulate organic carbon from the Himalaya to the Ganga–Brahmaputra delta. *Geochimica et Cosmochimica Acta*, *72*(7), 1767–1787. https://doi.org/10.1016/j.gca.2008.01.027

Garzanti, E., Andó, S., France-Lanord, C., Censi, P., Vignola, P., Galy, V., & Lupker, M. (2011). Mineralogical and chemical variability of fluvial sediments 2. Suspended-load silt (Ganga–Brahmaputra, Bangladesh). *Earth and Planetary Science Letters*, *302*(1), 107–120. https://doi.org/10.1016/j.epsl.2010.11.043

Girling, C. A. (1984). Selenium in agriculture and the environment. *Agriculture, Ecosystems & Environment*, *11*(1), 37–65. https://doi.org/10.1016/0167-8809(84)90047-1

Hale, R., Bain, R., Goodbred Jr., S., & Best, J. (2019). Observations and scaling of tidal mass transport across the lower Ganges–Brahmaputra delta plain: Implications for delta management and sustainability. *Earth Surface Dynamics*, *7*(1), 231–245. https://doi.org/10.5194/esurf-7-231-2019

Hatje, V., Payne, T. E., Hill, D. M., McOrist, G., Birch, G. F., & Szymczak, R. (2003). Kinetics of trace element uptake and release by particles in estuarine waters: Effects of pH, salinity, and particle loading. *Environment International*, *29*(5), 619–629. https://doi.org/10.1016/S0160-4120(03)00049-7

Islam, M. A., Al-mamun, A., Hossain, F., Quraishi, S. B., Naher, K., Khan, R., Das, S., Tamim, U., Hossain, S. M., & Nahid, F. (2017). Contamination and ecological risk assessment of trace elements in sediments of the rivers of Sundarban mangrove forest, Bangladesh. *Marine Pollution Bulletin*, *124*(1), 356–366. https://doi.org/10.1016/j.marpolbul.2017.07.059

Jayaram, C., Roy, R., Chacko, N., Swain, D., Punnana, R., Bandyopadhyay, S., ... & Dutta, D. (2021). Anomalous Reduction of the Total Suspended Matter During the COVID-19 Lockdown in the Hooghly Estuarine System. *Frontiers in Marine Science*, 8, 633493. https://doi.org/10.3389/fmars.2021.633493

Jeandel, C., & Oelkers, E. H. (2015). The influence of terrigenous particulate material dissolution on ocean chemistry and global element cycles. *Chemical Geology*, *395*, 50–66. https://doi.org/10.1016/j.chemgeo.2014.12.001

Khan, M. M. H., Bryceson, I., Kolivras, K. N., Faruque, F., Rahman, M. M., & Haque, U. (2015). Natural disasters and land-use/land-cover change in the southwest coastal areas of

Bangladesh. *Regional Environmental Change*, *15*(2), 241–250. https://doi.org/10.1007/s10113-014-0642-8

Kibria, G., Hossain, M. M., Mallick, D., Lau, T. C., & Wu, R. (2016). Monitoring of metal pollution in waterways across Bangladesh and ecological and public health implications of pollution. *Chemosphere*, *165*, 1–9. https://doi.org/10.1016/j.chemosphere.2016.08.121

Kosmulski, M. (2018). The pH dependent surface charging and points of zero charge. VII. Update. *Advances in Colloid and Interface Science*, *251*, 115–138. https://doi.org/10.1016/j.cis.2017.10.005

Kumar, A., Ramanathan, AL., Prasad, M. B. K., Datta, D., Kumar, M., & Sappal, S. M. (2016). Distribution, enrichment, and potential toxicity of trace metals in the surface sediments of Sundarban mangrove ecosystem, Bangladesh: A baseline study before Sundarban oil spill of December, 2014. *Environmental Science and Pollution Research*, *23*(9), 8985–8999. https://doi.org/10.1007/s11356-016-6086-6

Li, Y.-H., Burkhardt, L., & Teraoka, H. (1984). Desorption and coagulation of trace elements during estuarine mixing. *Geochimica et Cosmochimica Acta*, *48*(10), 1879–1884. https://doi.org/10.1016/0016-7037(84)90371-5

Lindsay, J. F., Holliday, D. W., & Hulbert, A. G. (1991). Sequence stratigraphy and the evolution of the Ganges-Brahmaputra Delta complex. *AAPG bulletin*, *75*(7), 1233-1254.

Lupker, M., France-Lanord, C., Galy, V., Lavé, J., Gaillardet, J., Gajurel, A. P., Guilmette, C., Rahman, M., Singh, S. K., & Sinha, R. (2012). Predominant floodplain over mountain weathering of Himalayan sediments (Ganga basin). *Geochimica et Cosmochimica Acta*, *84*, 410–432. https://doi.org/10.1016/j.gca.2012.02.001

Mason, R. (2013). Trace Metal(loid)s in Marine Waters. In *Trace Metals in Aquatic Systems* (pp. 219–309). John Wiley & Sons, Ltd. https://doi.org/10.1002/9781118274576.ch6

Millward, G. E., & Liu, Y. P. (2003). Modelling metal desorption kinetics in estuaries. *Science of The Total Environment*, *314–316*, 613–623. https://doi.org/10.1016/S0048-9697(03)00077-9

Moore, W. S. (1997). High fluxes of radium and barium from the mouth of the Ganges-Brahmaputra River during low river discharge suggest a large groundwater source. *Earth and Planetary Science Letters*, *150*(1), 141–150. https://doi.org/10.1016/S0012-821X(97)00083-6

Nickson, R. T., McArthur, J. M., Ravenscroft, P., Burgess, W. G., & Ahmed, K. M. (2000). Mechanism of arsenic release to groundwater, Bangladesh and West Bengal. *Applied Geochemistry*, *15*(4), 403–413. https://doi.org/10.1016/S0883-2927(99)00086-4

Rahaman, S. M. B., Sarder, L., Rahaman, M. S., Ghosh, A. K., Biswas, S. K., Siraj, S. S., Huq, K. A., Hasanuzzaman, A. F. M., & Islam, S. S. (2013). Nutrient dynamics in the Sundarbans mangrove estuarine system of Bangladesh under different weather and tidal cycles. *Ecological Processes*, *2*(1), 29. https://doi.org/10.1186/2192-1709-2-29

Rahaman, S. M., Biswas, S. K., Rahaman, M. S., Ghosh, A. K., Sarder, L., Siraj, S., & Islam, S. S. (2014). Seasonal nutrient distribution in the Rupsha-Passur tidal river system of the Sundarbans mangrove forest, Bangladesh. *Ecological Processes*, *3*(1), 18. https://doi.org/10.1186/s13717-014-0018-5

Rahman, M. M., Dong, Z., & Naidu, R. (2015). Concentrations of arsenic and other elements in groundwater of Bangladesh and West Bengal, India: Potential cancer risk. *Chemosphere*, *139*, 54–64. https://doi.org/10.1016/j.chemosphere.2015.05.051

Rosen, B. P., & Liu, Z. (2009). Transport pathways for arsenic and selenium: A minireview. *Environment International*, *35*(3), 512–515. https://doi.org/10.1016/j.envint.2008.07.023

Rudnick, R. L., & Gao, S. (2003). Composition of the Continental Crust. *Treatise On Geochemistry*, *3*, 1–64.

Samanta, S., & Dalai, T. K. (2016). Dissolved and particulate Barium in the Ganga (Hooghly) River estuary, India: Solute-particle interactions and the enhanced dissolved flux to the oceans. *Geochimica et Cosmochimica Acta*, *195*, 1–28. https://doi.org/10.1016/j.gca.2016.09.005

Samanta, S., & Dalai, T. K. (2018). Massive production of heavy metals in the Ganga (Hooghly) River estuary, India: Global importance of solute-particle interaction and enhanced metal fluxes to the oceans. *Geochimica et Cosmochimica Acta*, *228*, 243–258. https://doi.org/10.1016/j.gca.2018.03.002

Spallholz, J. E., Mallory Boylan, L., & Rhaman, M. M. (2004). Environmental hypothesis: Is poor dietary selenium intake an underlying factor for arsenicosis and cancer in Bangladesh and West Bengal, India? *Science of The Total Environment*, *323*(1), 21–32. https://doi.org/10.1016/j.scitotenv.2003.09.034

Strady, E., Dinh, Q. T., Némery, J., Nguyen, T. N., Guédron, S., Nguyen, N. S., Denis, H., & Nguyen, P. D. (2017). Spatial variation and risk assessment of trace metals in water and sediment of the Mekong Delta. *Chemosphere*, *179*, 367–378. https://doi.org/10.1016/j.chemosphere.2017.03.105

Thanh-Nho, N., Strady, E., Nhu-Trang, T., David, F., & Marchand, C. (2018). Trace metals partitioning between particulate and dissolved phases along a tropical mangrove estuary

(Can Gio, Vietnam). *Chemosphere*, *196*, 311–322. https://doi.org/10.1016/j.chemosphere.2017.12.189

U.S. EPA [U.S. Environmental Protection Agency]. (2009). *National Primary Drinking Water Regulations*. https://www.epa.gov/sites/production/files/2016-06/documents/npwdr_complete_table.pdf

Wang, W., & Wang, W.-X. (2016). Phase partitioning of trace metals in a contaminated estuary influenced by industrial effluent discharge. *Environmental Pollution*, *214*, 35–44. https://doi.org/10.1016/j.envpol.2016.03.059

Weng, N., & Wang, W.-X. (2014). Variations of trace metals in two estuarine environments with contrasting pollution histories. *Science of The Total Environment*, *485–486*, 604–614. https://doi.org/10.1016/j.scitotenv.2014.03.110

Williams, P. N., Islam, S., Islam, R., Jahiruddin, M., Adomako, E., Soliaman, A. R. M., Rahman, G. K. M. M., Lu, Y., Deacon, C., Zhu, Y.-G., & Meharg, A. A. (2009). Arsenic Limits Trace Mineral Nutrition (Selenium, Zinc, and Nickel) in Bangladesh Rice Grain. *Environmental Science & Technology*, *43*(21), 8430–8436. https://doi.org/10.1021/es901825t

Winkel, L. H. E., Johnson, C. A., Lenz, M., Grundl, T., Leupin, O. X., Amini, M., & Charlet, L. (2012). Environmental Selenium Research: From Microscopic Processes to Global Understanding. *Environmental Science & Technology*, *46*(2), 571–579. https://doi.org/10.1021/es203434d

Wright, J., & Colling, A. (1995). *Seawater: Its Composition, Properties and Behaviour*. Elsevier. https://doi.org/10.1016/C2013-0-10208-5

ELEMENT TRANSPORT AND PARTITIONING ALONG TIDAL CHANNELS IN SOUTHWEST BANGLADESH

Supporting Information

Authors: Matthew Dietrich[a1] and John C. Ayers[a]

[a]Department of Earth and Environmental Sciences, Vanderbilt University, 5726 Stevenson Center, 7th floor, Nashville, TN 37240, United States

[1]Corresponding Author: mjdietri@iu.edu

Text B1—Sample incubation time correlation results and suspended vs dissolved load concentrations

There are mostly poor linear trends with significant scatter between element concentrations in the suspended and the dissolved load (Fig. B10). When comparing the lab filtered samples (0.2 µm) in this study with duplicates filtered in the field (0.45 µm) from a companion study (Dietrich & Ayers, 2021), Co and Ni in the lab filtered samples are significantly elevated in concentration, along with Cr, Zn and Cu (Fig. B11). Most other elements are similar in concentration. Additionally, Co and Ni have slight negative trends between the dissolved and solid load concentrations (Fig. B10). No trends are seen between Co and Ni Kd values and time from sampling to filtration (Fig. B12). There is little correlation between days from sampling to filtration and concentrations of almost all elements in the dissolved and solid load except for Se, Mn, Cr, and V in the dissolved load (Figs. B4 & B5). An element of interest in this study, Se, does show a moderate negative correlation between days from sampling to filtration and dissolved concentration (Fig. B13).

Text B2—Discussion of possible effects of sample incubation time on the geochemistry of samples and interpretation of results

Most trace elements that may undergo desorption or dissolution processes showed significant scatter between the dissolved and suspended loads, suggesting disequilibrium partitioning (Fig. B10). Thus, even though the suspended sediments were in contact with the water for an extended period of time, slow kinetics likely prevented exchange equilibrium and any changes in water or sediment concentration were likely less than an order of magnitude. Because many of our interpretations are based on geochemical changes greater than an order of magnitude (i.e., Kd values and dissolved concentrations of Se), any sample incubation effects were likely less than the observed changes. Also, the residence time of water in the tidal channel during which reactions between sediment and water can occur was likely similar in magnitude to sample incubation time, because most water in this area is tidally reworked (Hale et al., 2019). Thus, any alterations to water and sediment chemistry from their interactions with one another likely occurred prior to our sampling and laboratory storage, especially because the salinity front in the dry season extends north past Khulna and our sampling area, where our samples first experienced freshwater-saltwater interactions and possible ionic exchange. Lastly, because of the highly saline nature of the waters, lack of significant headspace in the sealed samples during storage, sample refrigeration for the majority of sample storage time, and relatively low DOC compared to world rivers (Gaillardet et al., 2014), biological reactions were also likely limited. This was additionally shown by poor correlation between DOC and days from sampling to filtration (Fig. B4).

Specifically regarding Ni and Co Kd values, the lack of any trends with days from sampling to filtration (Fig. B12) suggests that the desorption from salt cations occurred predominantly before the samples were stored or in the early stages of storage, which would resemble real-world processes of increased residence time from additional tidal reworking or irrigation into ponds. Apparent Kd values would have the highest uncertainties for elements affected by sample incubation because concentrations in water and sediment change in opposite directions. Post-sampling effects of Se however, are possible, although there is lack of sufficient evidence to conclude that a significant amount of Se was sorbed, desorbed, or co-precipitated on suspended sediment during sample storage. The first line of insufficient evidence is the lack of exchange equilibrium between measurable dissolved and suspended Se (Fig. B10). Second, there is only a slight negative correlation ($r^2 = 0.48$; Fig. B13) between dissolved Se and the days from sampling to filtration. If there was a strong effect on the dissolved Se during sample storage, one would expect the correlation to be stronger, particularly if Se ranged 2 orders of magnitude in the dissolved load (Table 2). Third, when excluding four samples from the separate "non-effluent" 24-hour sampling period, Se is more strongly linearly correlated with salinity ($r^2 = 0.76$) relative to days from sampling to filtration ($r^2 = 0.25$), implying the trends are indeed from mixing with seawater and not induced by sample incubation. Lastly, Se concentrations in duplicate samples filtered in the field for samples MD-TC-18 and MD-TC-19 were 15 µg/L and 30 µg/L, respectively, both less than any lab-filtered samples in this study taken during the proposed 24-hour effluent release event. Thus, even if some of the dissolved Se became immobilized in the solid phase during incubation (as suggested by the negative correlation between dissolved Se and days to filtering), the dissolved concentrations from the field filtrations (taken in the second, "non-effluent" 24-hr period) are still lower than all the Se concentrations in the main 24-hr

sampling period, supporting our Se anthropogenic effluent interpretations. However, slight sorption/desorption or coprecipitation of Se during sample storage cannot be fully discounted, particularly because of the differences in concentrations of Se in duplicate field filtered and lab filtered samples (Fig. B11) and that several other redox sensitive metals (Cr, V, and Mn) showed moderate negative correlations with days from sampling to filtration (Fig. B4).

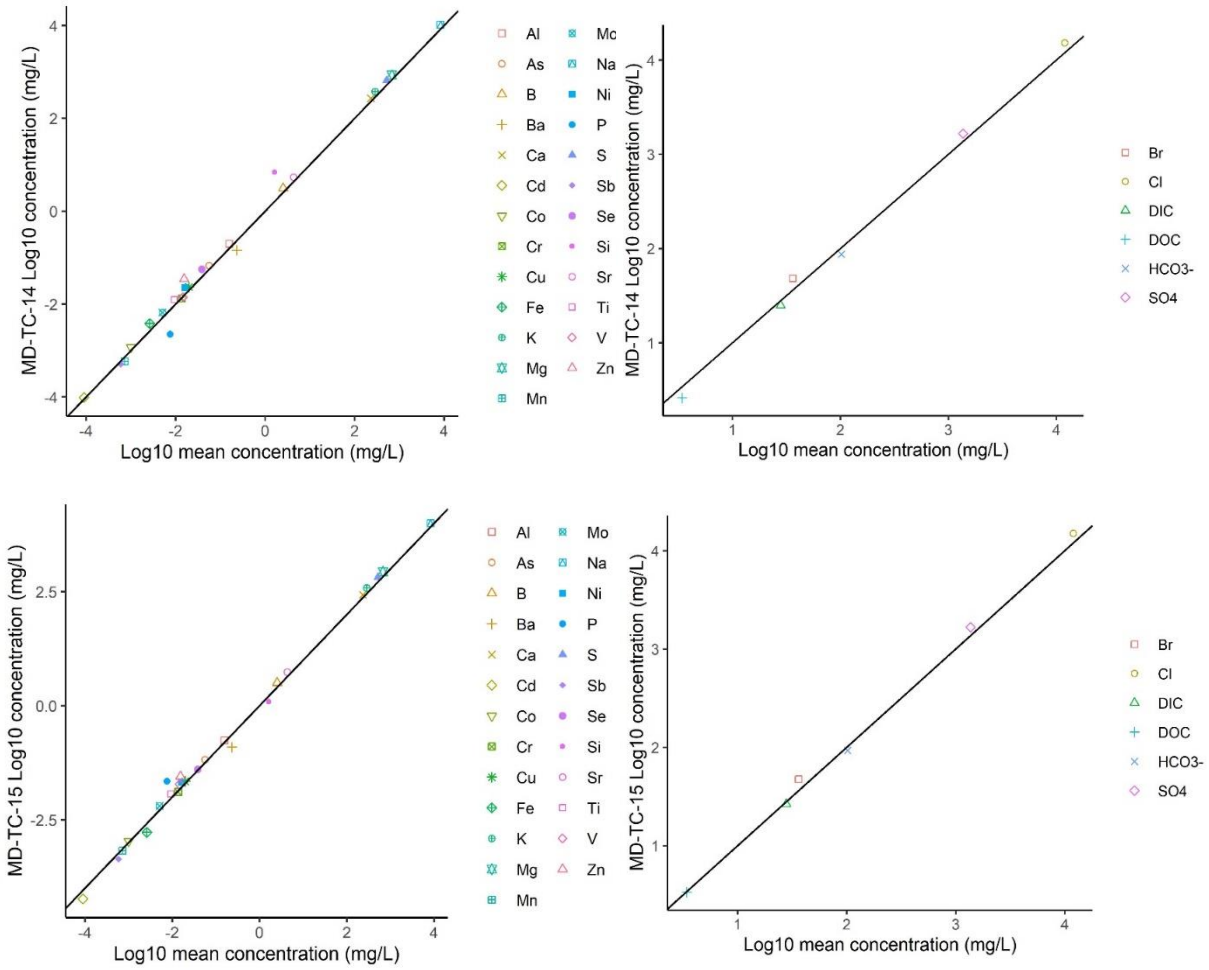

Figure B1: Log10 element concentrations in metal buckets versus log10 mean concentrations of elements in plastic buckets, with a 1:1 ratio line inserted in black.

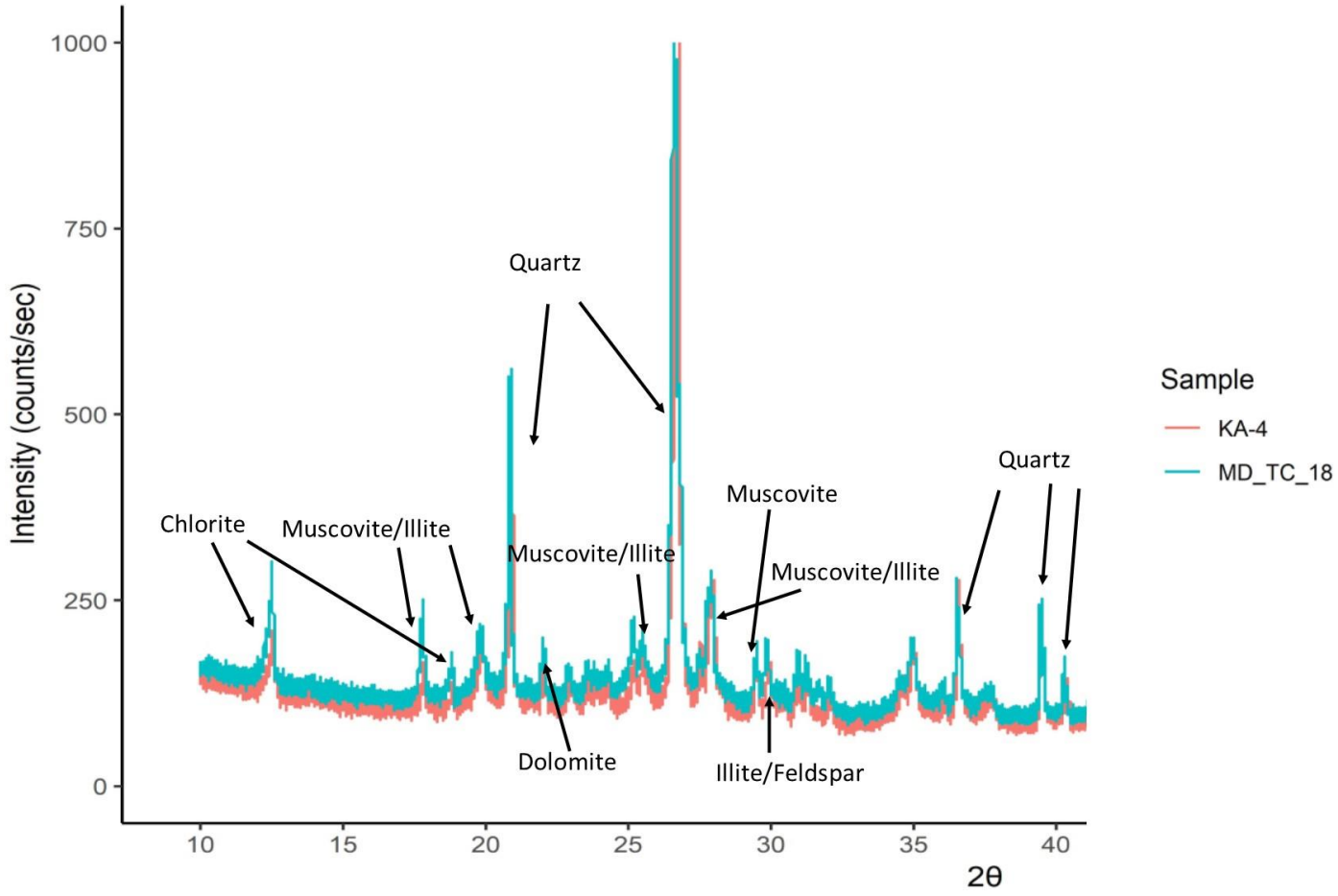

Figure B2: Powder XRD analysis of suspended sediment (>2.5µm) in the upper 1m of a tidal channel (MD-TC-18) and a shrimp pond sediment sample (Location KA-4; Dietrich and Ayers, 2021) in Southwest Bangladesh. Major mineral phases are identified with their corresponding peaks. Feldspar is a K-component of Feldspar – K (Al Si3 O8). The y-axis depicts observed intensity and is truncated for better visualization.

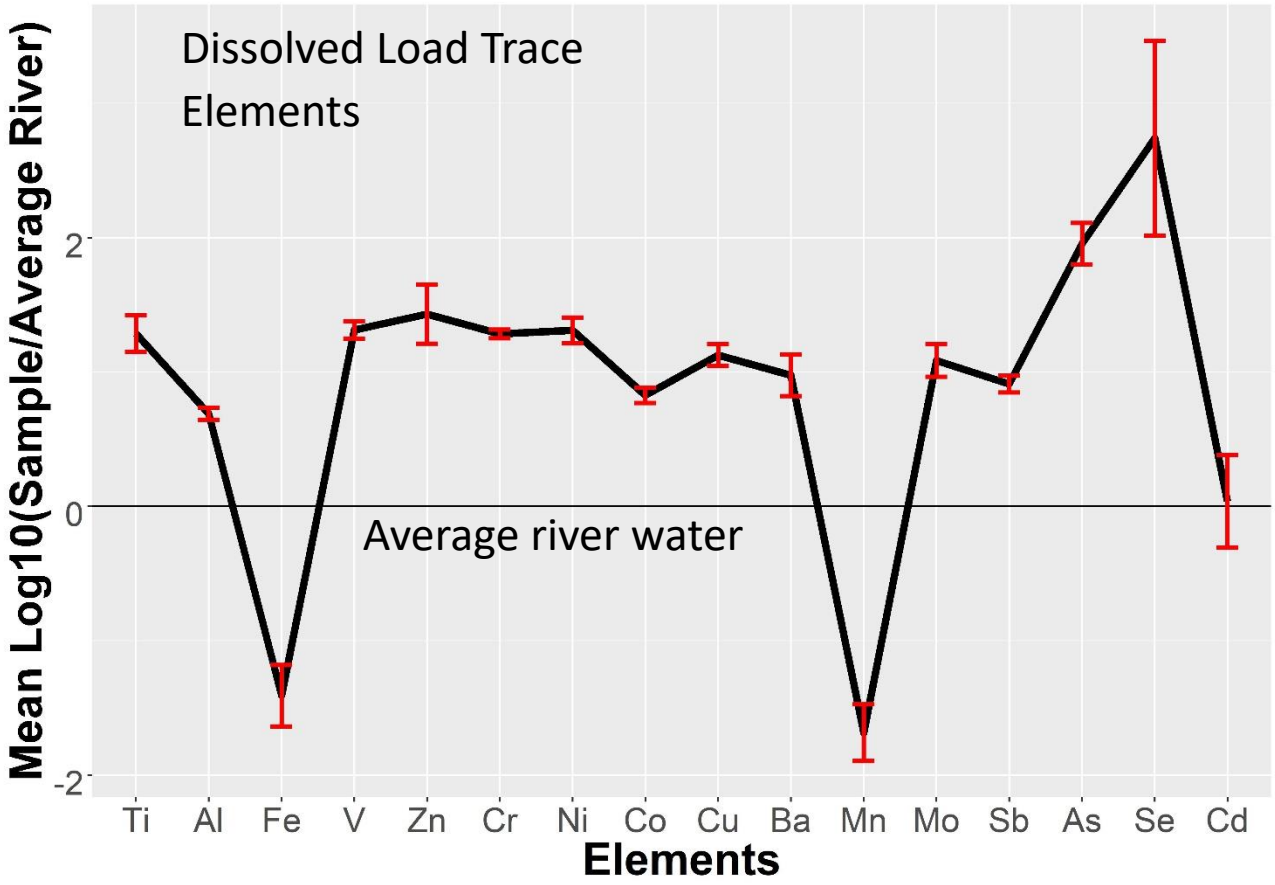

Figure B3: Dissolved element concentrations normalized to average riverine element concentrations (Gaillardet et al., 2014) with 1σ variation error bars.

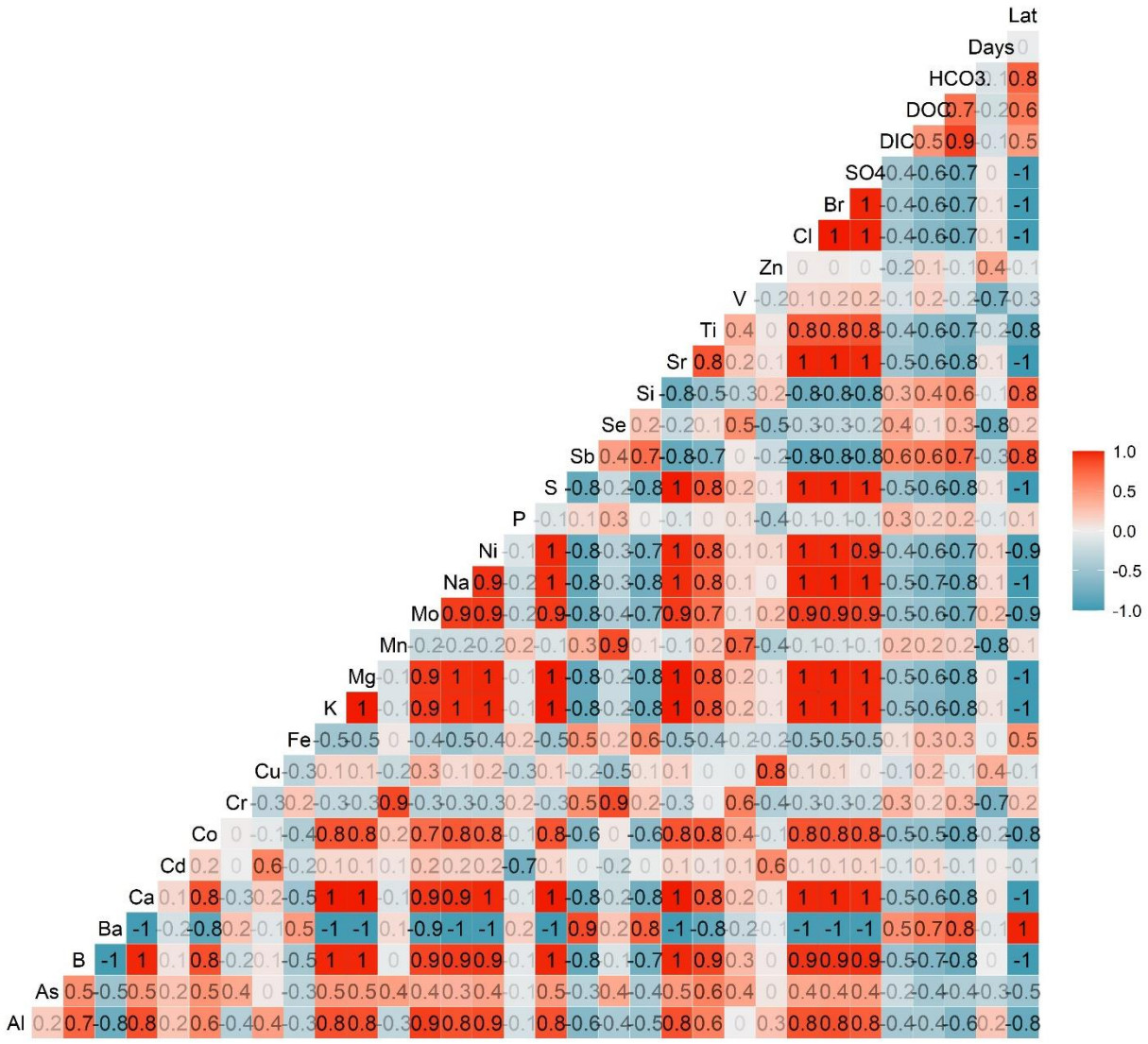

Figure B4: Dissolved load Spearman Rank correlation matrix (several elements are non-normally distributed) with color bar scale. "Days" stands for days from sampling to lab filtration and "Lat" for latitude. The MDL for one negative P reported concentration was inserted.

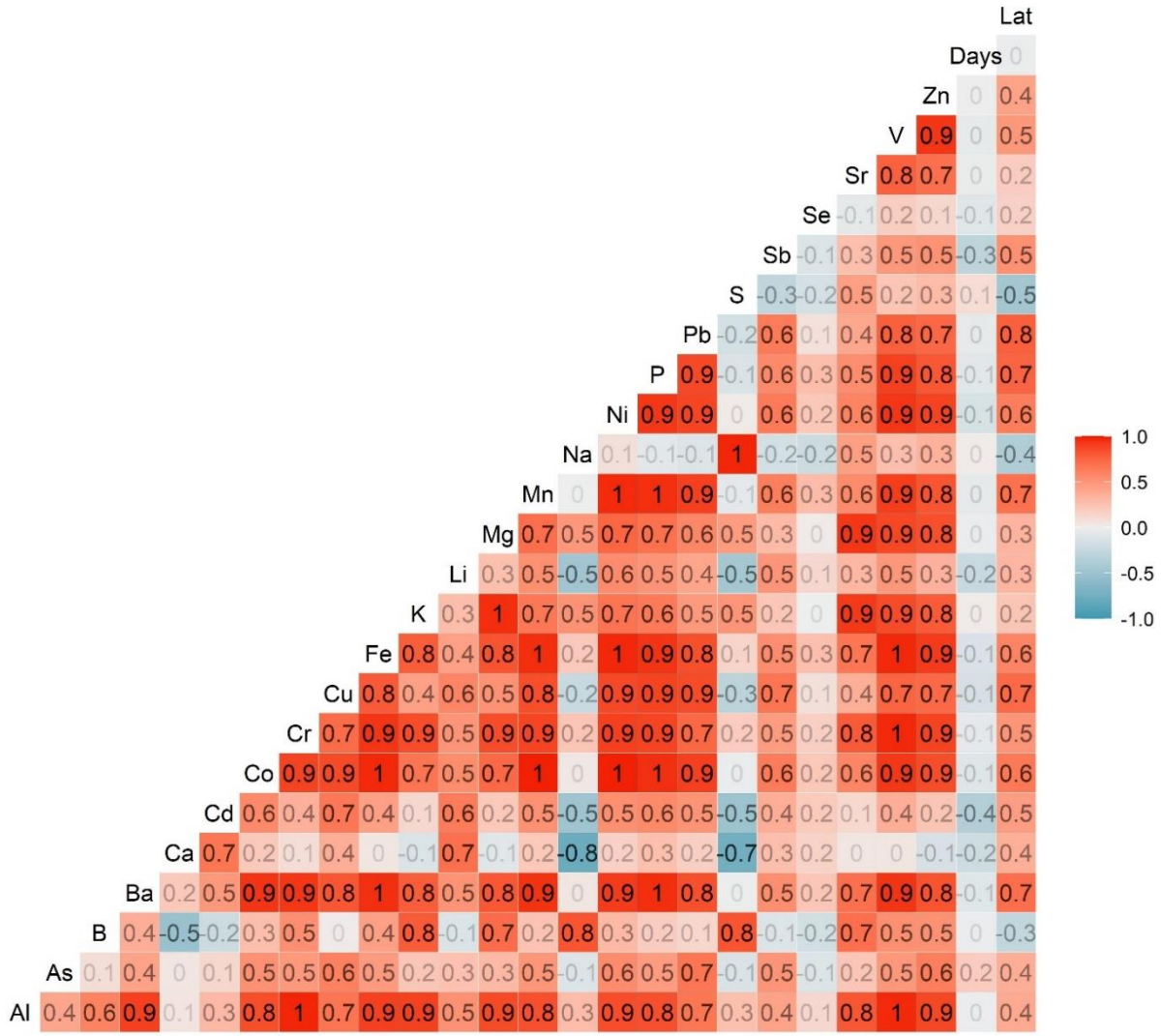

Figure B5: Suspended sediment load Spearman Rank correlation matrix (several elements are non-normally distributed) with color bar scale (detection limit values substituted in for element values <MDL). "Days" stands for days from sampling to lab filtration and "Lat" for latitude.

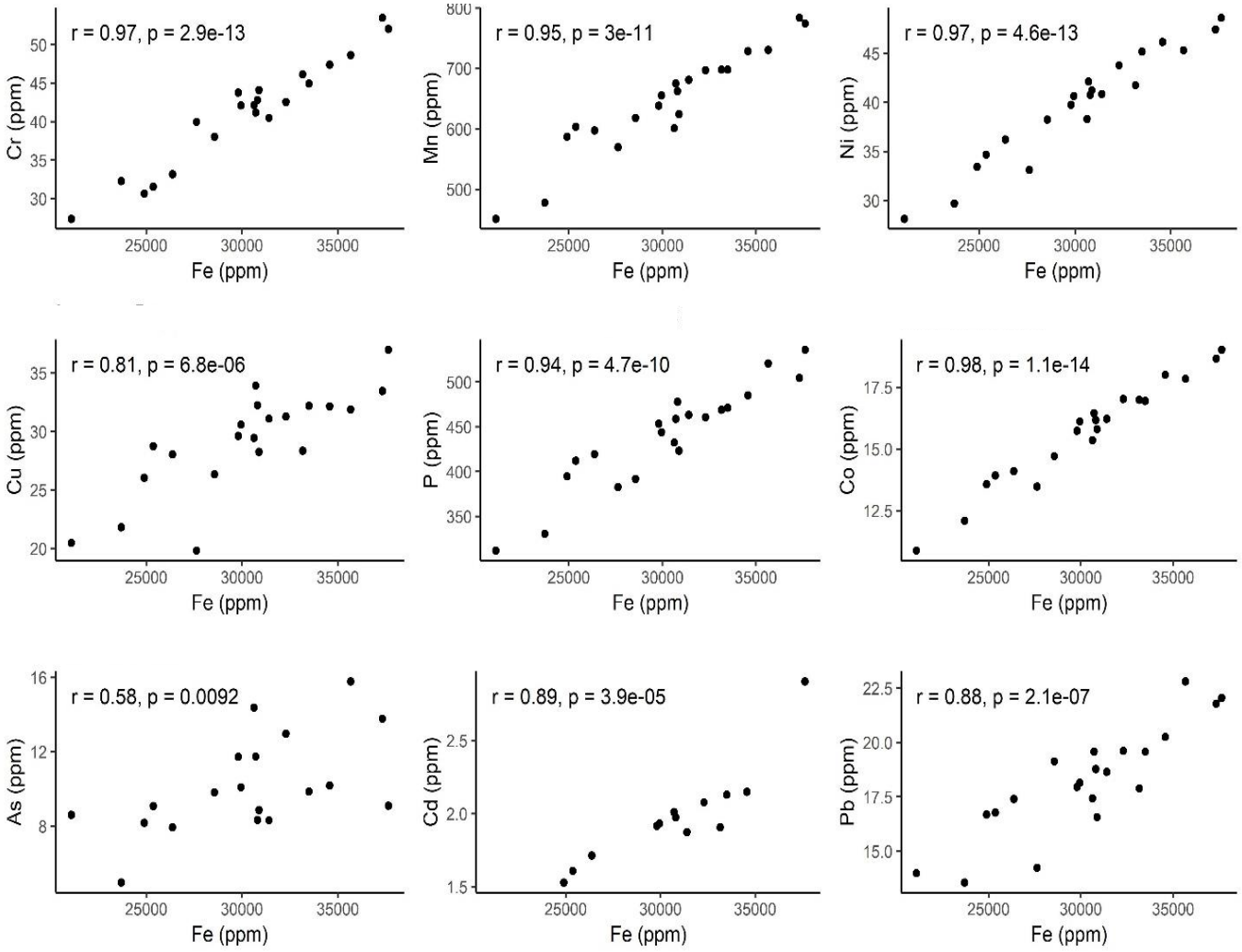

Figure B6: Several elements that showed significant positive correlations with Fe in the suspended sediment load. Concentrations <MDL are excluded. Pearson correlation coefficients and p-values are given.

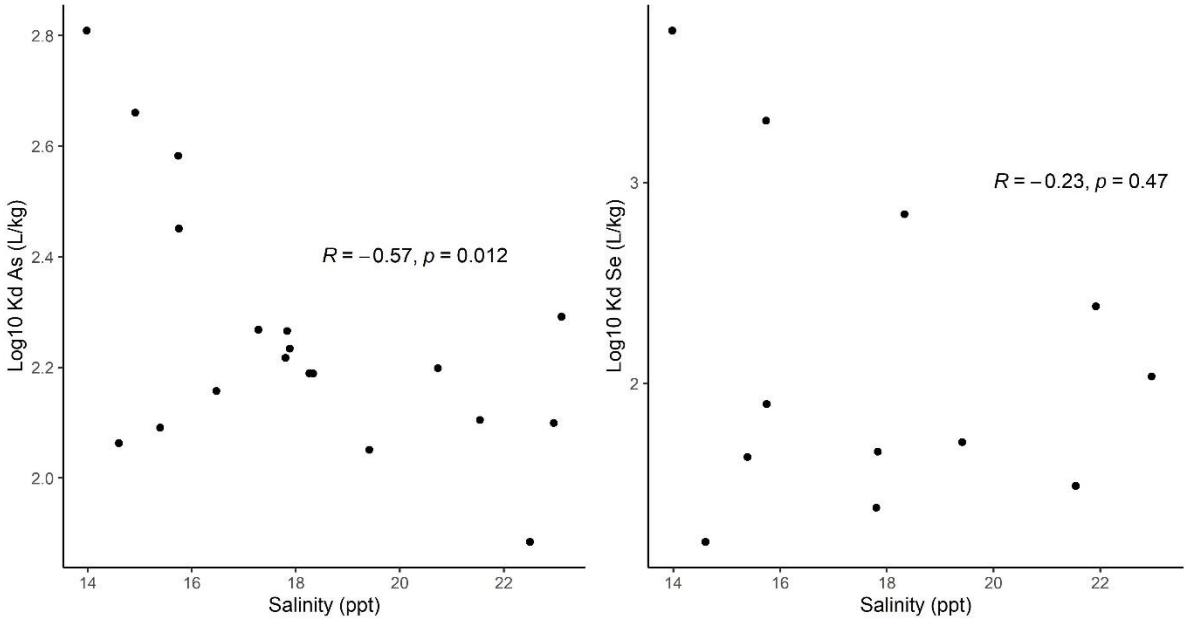

Figure B7: Salinity trends of As and Se Kd values in Log10 (L/kg) (results <MDL excluded) along the transect with increased seawater mixing. Pearson correlation coefficients and p-values are given.

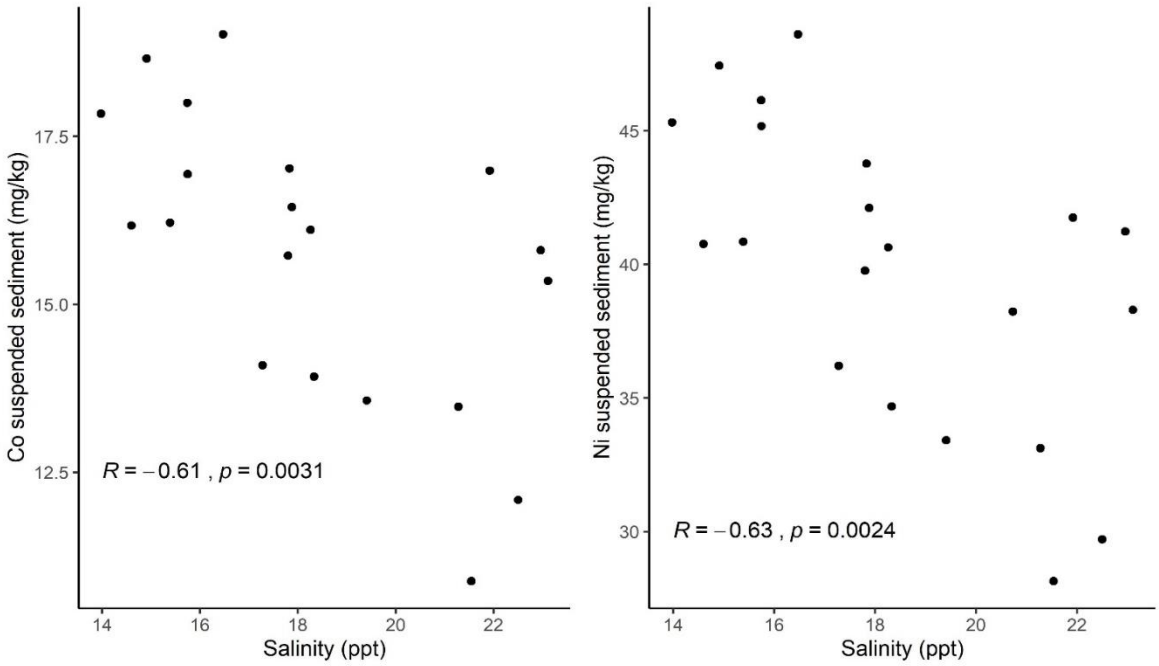

Figure B8: Cobalt and nickel suspended sediment concentration plotted against salinity, with Pearson correlation coefficients and p-values.

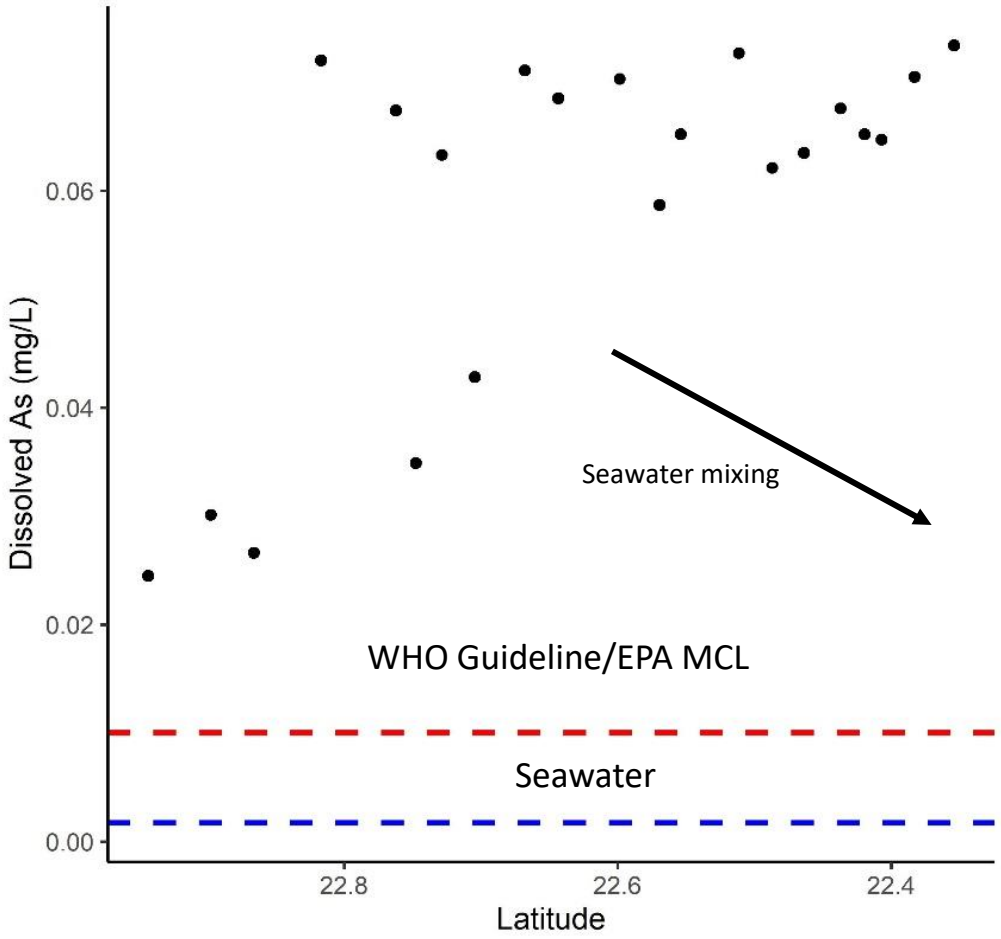

Figure B9: Dissolved As versus latitude. Correlation coefficients are ommitted because of the anchoring effect of the three high latitude values in the Bhairab River. Large scatter with no definitive trend is apparent between all other samples. Average open seawater As is 0.0017 mg/L (Mason, 2013) and is marked by the blue dashed line, while the WHO guideline/EPA MCL (0.01 mg/L) is marked by the red dashed line.

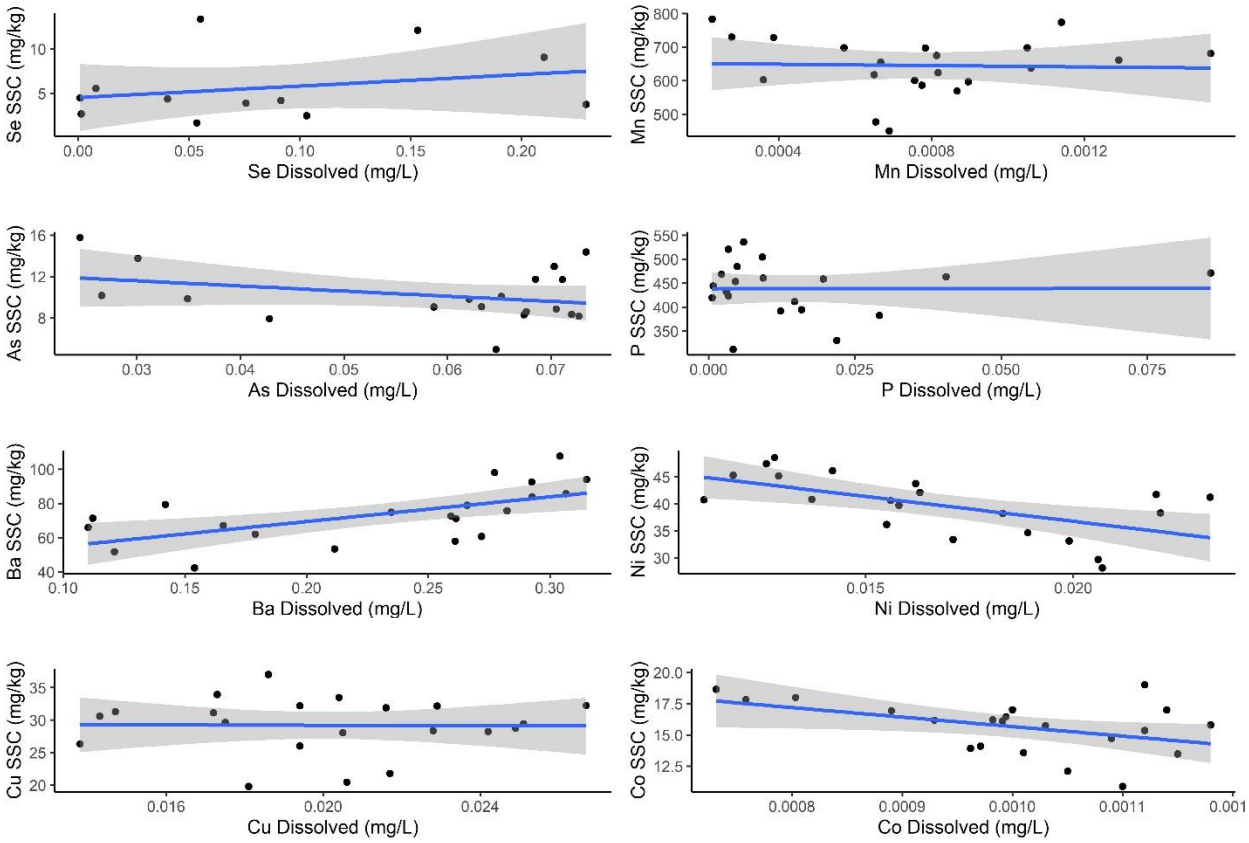

Figure B10: Element concentrations in the suspended sediment (SSC) load versus concentrations in the dissolved load. Values <MDL are omitted. The shaded gray regions represent the 95% confidence interval about the linear regression line, with linear regression statistics omitted because of the large scatter in the data (as seen with large confidence intervals).

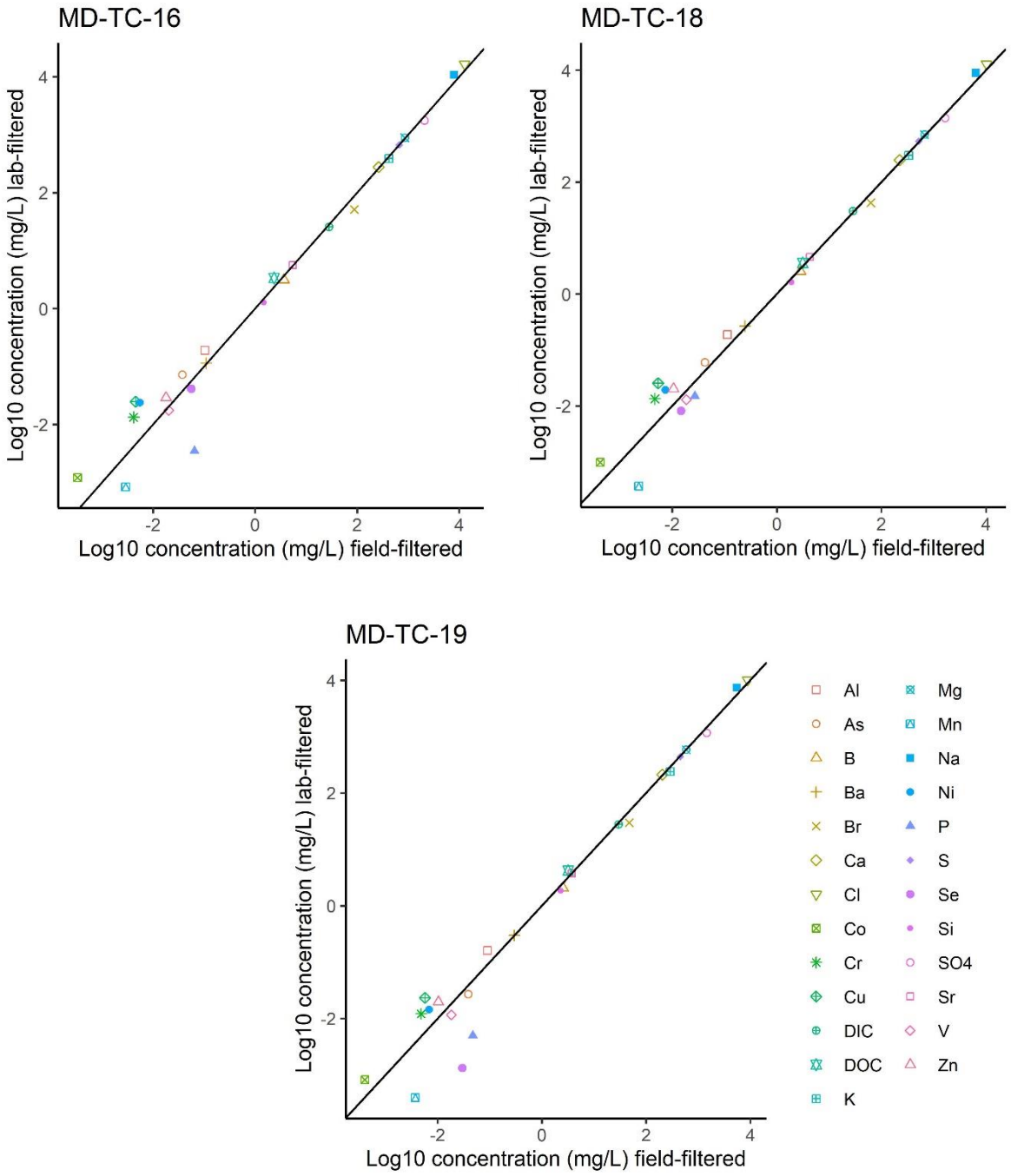

Figure B11: Comparison of field filtered dissolved load concentrations (0.45µm; Dietrich and Ayers, 2021) with lab filtered dissolved concentrations (0.2 µm; This study). Each set of samples were at the same study site. Black lines are for 1:1 comparison between sample types, with a slope of 1 and y-intercept of 0. Samples falling on the black line indicate the same concentrations in both sets of samples.

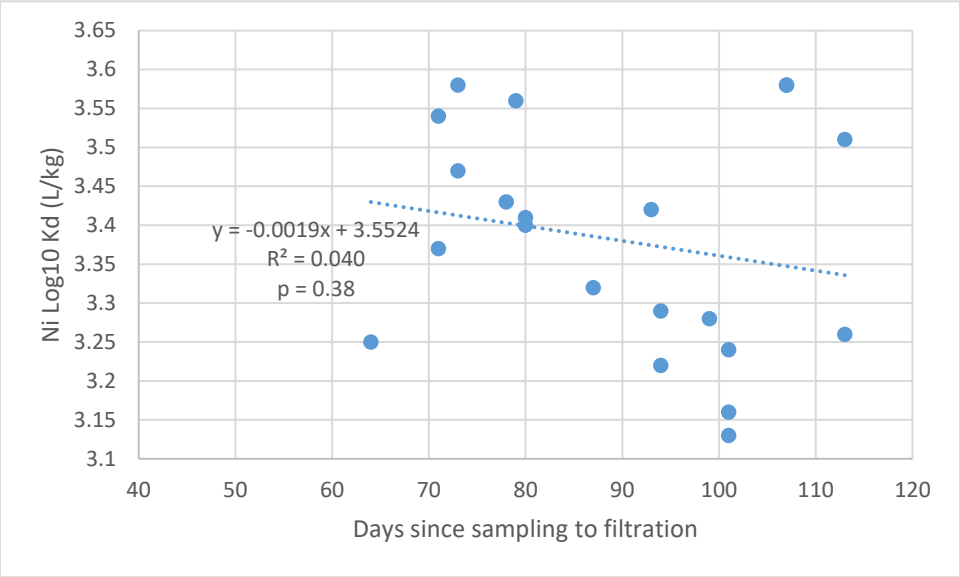

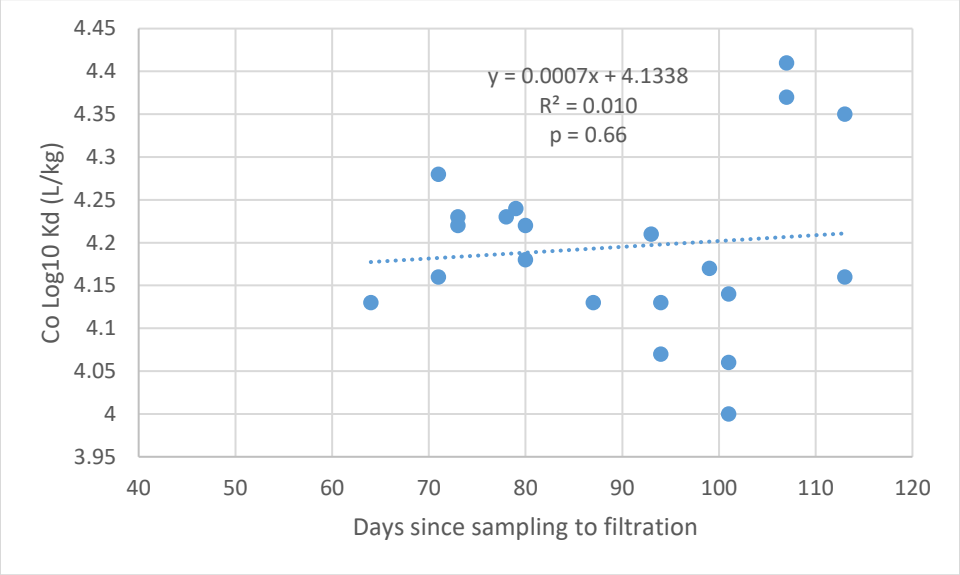

Figure B12: Days since sampling to lab filtration versus Co and Ni Kd values. Linear regression lines are provided.

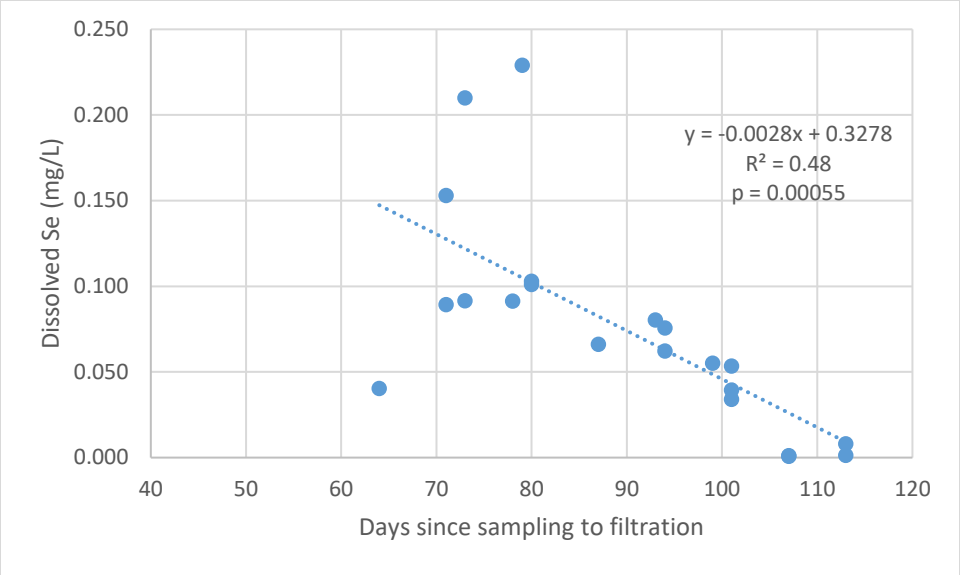

Figure B13: Days since sampling to lab filtration versus the dissolved Se concentration. The linear regression line is provided.

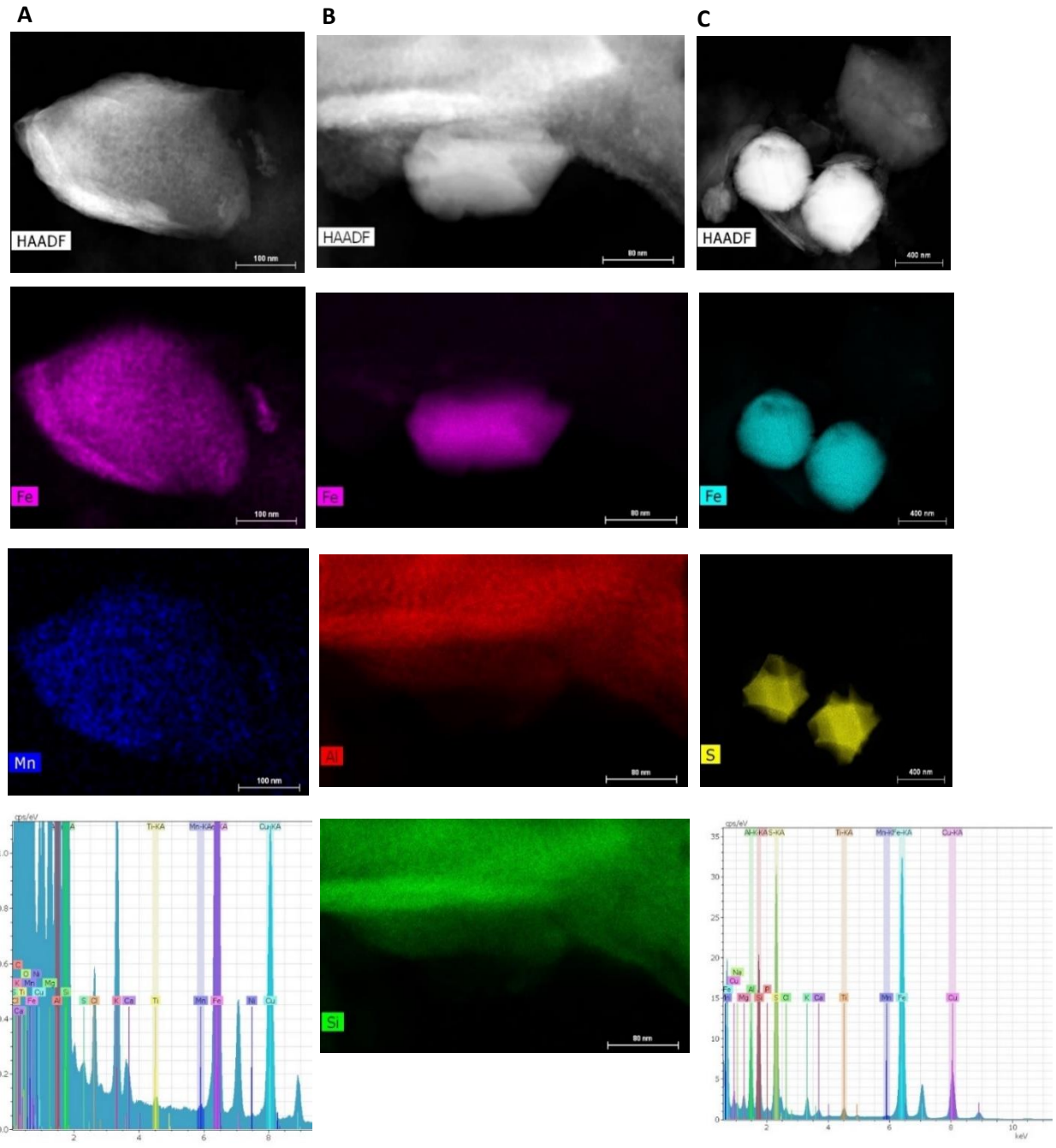

Figure B14: TEM analysis of several Fe-rich particles from samples MD-TC-7 (first two columns) and MD-TC-11 (third column), specifically showing: Column (**A**) – High-angle annular dark-field (HAADF) image, STEM-EDS maps, and EDS spectra with several element peaks identified for an Fe-rich particle (about 0.5 µm in diameter) associated with several transition metals such as Mn, Ti, Cu, and potentially Ni; Column (**B**) – HAADF image and STEM-EDS maps of Al, Si and Fe, showing the Fe-rich nanoparticle (~0.2 µm in diameter) associated with the larger aluminum silicate particle; Column (**C**) – HAADF image, STEM-EDS maps and EDS spectra, showing an Fe-sulfide particles ~0.5µm in diameter.

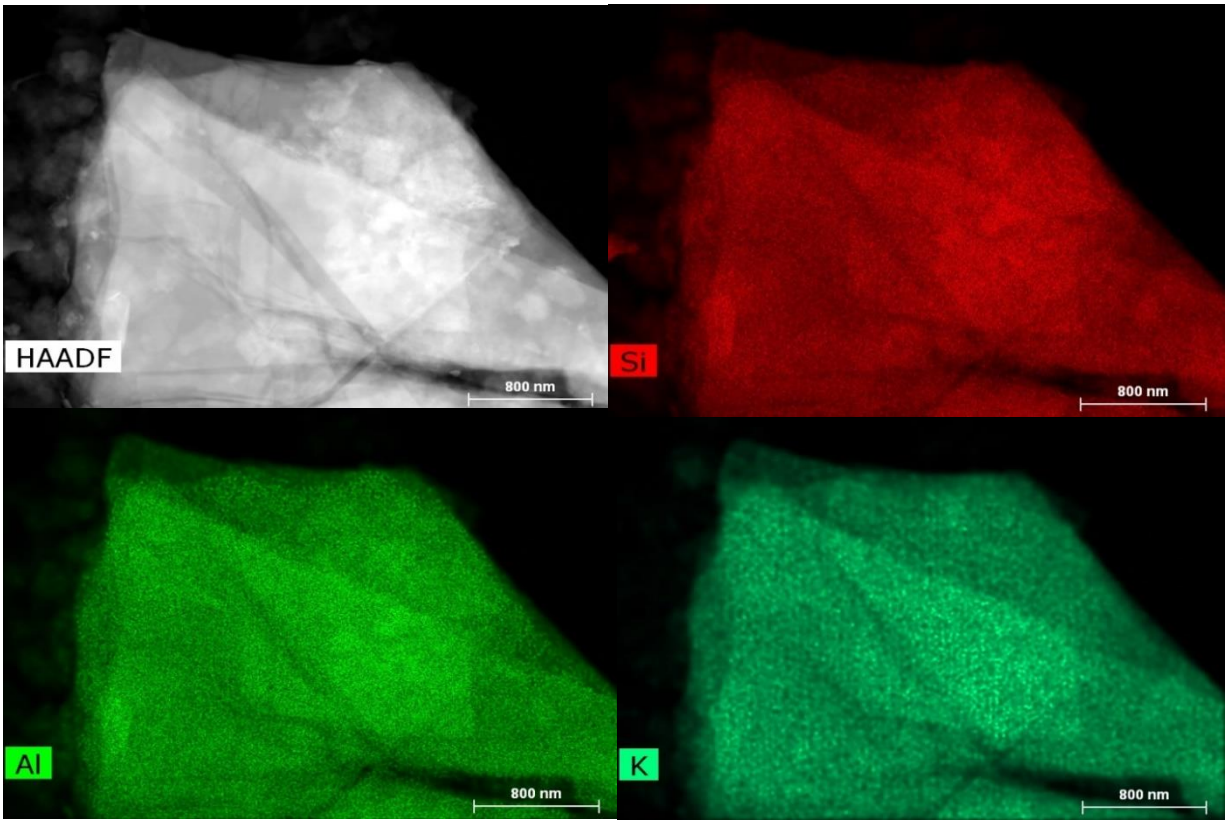

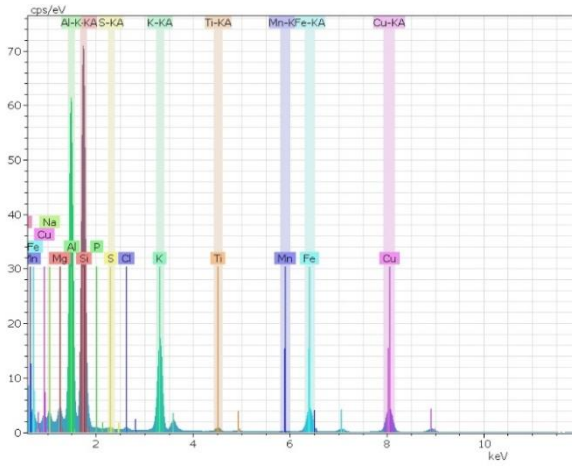

Element	series	Net	[wt.%]	[norm. wt.%]	[norm. at.%]	Error in wt.% (3 Sigma)
Silicon	K-series	298063	27.35	27.35	21.33	0.23
Aluminium	K-series	250267	22.88	22.88	18.57	2.14
Potassium	K-series	104185	9.93	9.93	5.56	0.97
Oxygen	K-series	447671	39.84	39.84	54.54	3.67
		Sum:	100	100	100	

Figure B15: TEM imaging of a K-silicate particle, potentially muscovite with other small crystals/oxides present, from sample MD-TC-11 with: a high-angle annular dark-field (HAADF) image, STEM-EDS maps, EDS spectra, and approximate wt.% and at. % concentrations of major elements present, assuming other contributions are relatively negligible.

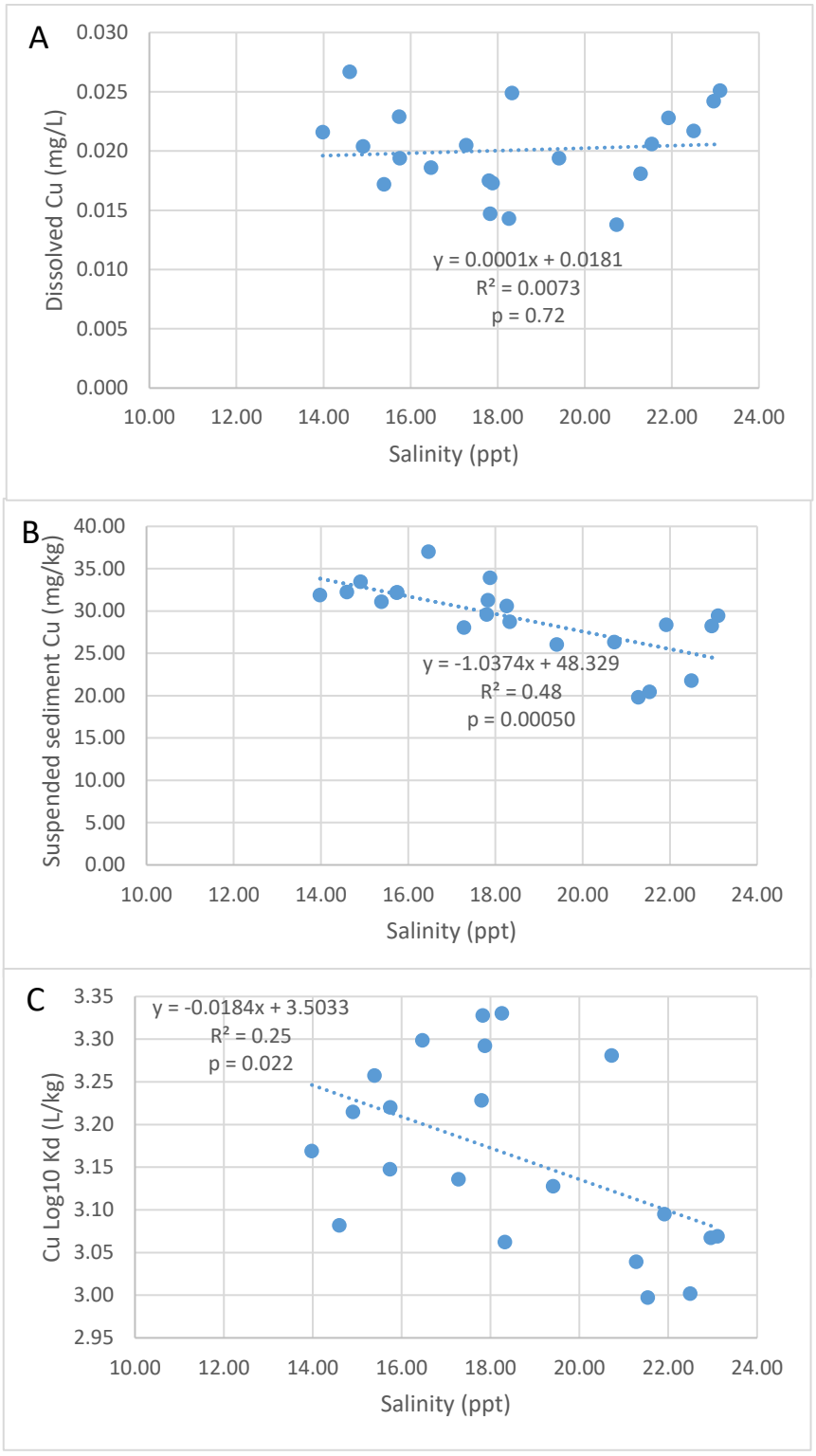

Figure B16: Dissolved (A), solid-phase suspended sediment (B), and Kd values of Cu (C) plotted against salinity. Linear regression lines are provided for each plot.

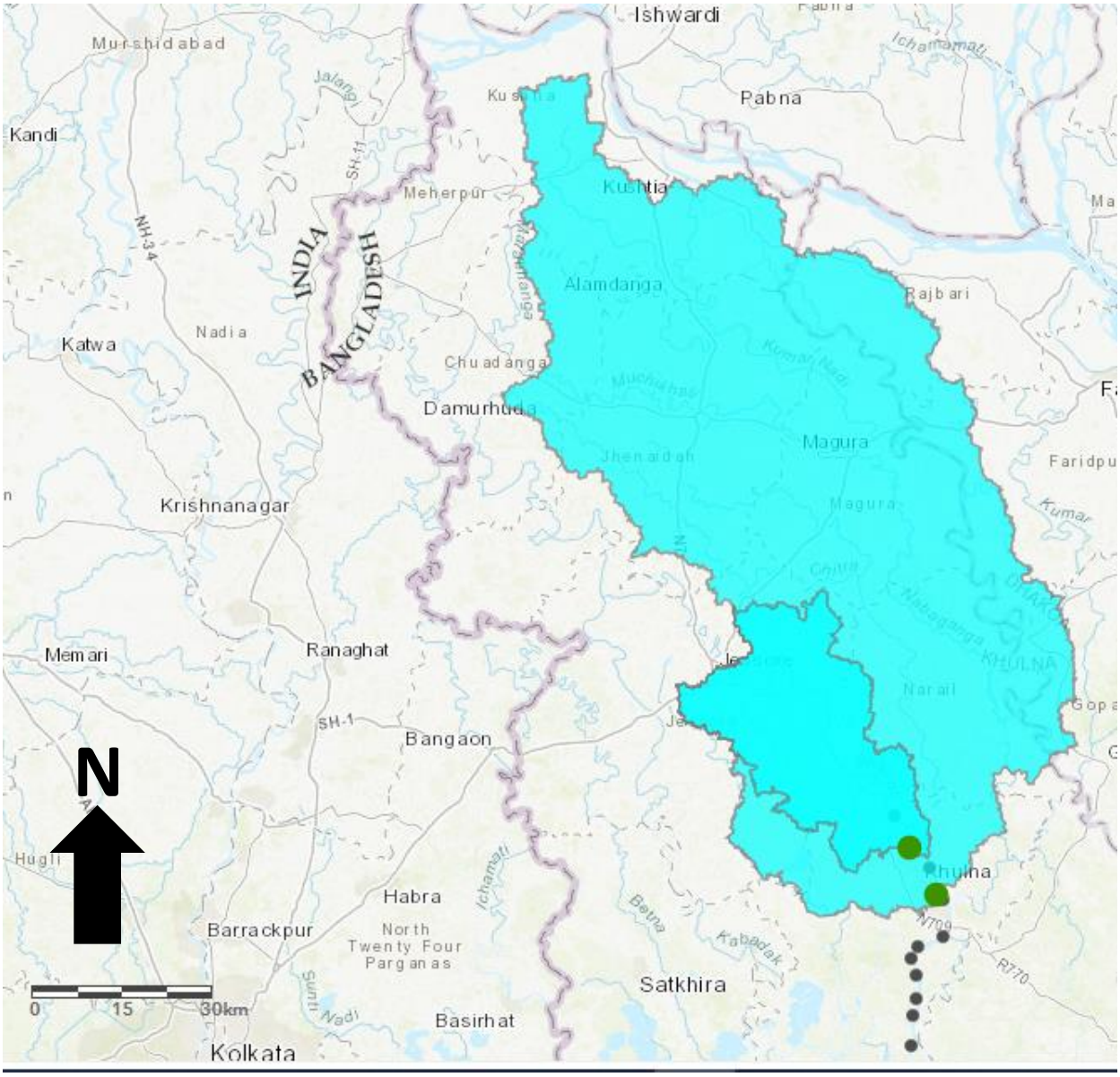

Figure B17: Watershed map for samples north of Khulna along the Bhairab River (smaller outlined watershed) and for samples south of Khulna along the Rupsha River (larger outlined watershed). Several sample sites are depicted as black dots, and the green dots represent the watershed drainage point.

Table B1: NIST standards 1646a (estuarine sediment) and 2702 (inorganics in marine sediment) run in duplicate on the ICP-OES under EPA Method 3051A to assess percent recovery of elements in sediments analgous to our suspended sediment samples. Percent recovery is only listed for elements that had either certified or reference mass fraction values listed within the standards.

Measured concentration (mg/kg)					% Recovery			
Element	**1646a_1**	**1646a_2**	**2702_1**	**2702_2**	**1646a_1**	**1646a_2**	**2702_1**	**2702_2**
Al	11080.0	11110.0	49690.0	50700.0	48.2	48.4	59.1	60.3
As	5.9	5.7	40.1	42.0	94.0	90.8	88.5	92.7
B	24.4	27.5	45.2	45.1				
Ba	37.0	35.9	162.2	167.8			40.8	42.2
Be	<0.851	<0.851	<0.851	<0.851				
Ca	3911.0	3966.0	2589.0	2632.0	75.4	76.4	75.5	76.7
Cd	1.0	1.1	4.5	4.6	704.1	728.4	554.0	566.7
Co	8.8	6.3	33.5	29.3			120.6	105.4
Cr	26.6	26.0	278.0	282.4	65.1	63.5	79.0	80.2
Cu	8.2	8.4	106.3	109.0	81.8	83.8	90.3	92.6
Fe	15810.0	16070.0	46480.0	47110.0	78.7	80.0		
K	3767.0	3735.0	12030.0	12360.0	43.6	43.2	58.6	60.2
Li	9.6	9.4	71.6	73.4				
Mg	3462.0	3469.0	8246.0	8529.0	89.2	89.4	83.3	86.2
Mn	164.8	165.8	1646.0	1682.0	70.3	70.7	93.7	95.7
Mo	1.2	1.0	7.1	6.7			65.6	62.3
Na	3994.0	4071.0	4140.0	4246.0	53.9	54.9	60.8	62.3
Ni	20.6	21.0	71.1	72.0			94.4	95.5
P	260.5	265.3	1397.0	1420.0	96.5	98.3	90.0	91.5
Pb	8.2	7.9	116.9	124.8	70.4	67.3	88.0	94.0
S	3203.0	3268.0	14380.0	14770.0	91.0	92.8		
Sb	<0.360	<0.360	7.1	6.7			126.4	120.3
Se	1.2	2.5	3.5	3.4	615.5	1296.9	69.8	68.7
Si	1862.0	1968.0	2368.0	2330.0	0.5	0.5		
Sr	24.0	23.8	64.2	67.1			53.6	56.1
Tl	<1.034	<1.034	<1.034	<1.034				
V	29.3	29.5	293.7	299.1	65.4	65.8	82.1	83.6
Zn	37.9	39.0	438.1	447.1	77.5	79.7	90.3	92.1

Table B2: Calculated Log10 Kd (bulk solid concentration/dissolved concentration) values (L/kg) used in this study (with MDLs used when suspended sediment values <MDL). The medians and standard deviations are also provided.

Sample ID	Al	Fe	V	Zn	Cr	Ni	Co	Cu	Ba	Mn	K	Ca	Sr	Na	Mg	Sb	As	Se	B	Cd	S
MD-TC-1	5.28	7.56	3.48	3.42	3.46	3.56	4.24	3.08	2.45	5.71	1.41	1.68	0.98	-0.15	1.36	3.36	2.06	1.21	0.63	4.28	0.31
MD-TC-2	5.23	6.75	3.45	3.78	3.40	3.47	4.22	3.26	2.43	5.65	1.38	1.46	0.91	-0.02	1.34	3.51	2.09	1.63	0.63	4.32	0.36
MD-TC-3	5.25	6.83	3.54	3.90	3.51	3.54	4.28	3.22	2.46	5.82	1.41	1.45	0.94	0.15	1.36	3.27	2.45	1.90	0.73	4.99	0.46
MD-TC-4	5.33	6.98	3.53	3.99	3.53	3.58	4.23	3.30	2.55	5.83	1.47	1.44	1.01	0.32	1.40	3.66	2.16	0.99	0.89	4.48	0.59
MD-TC-5	5.06	7.05	3.38	3.75	3.37	3.37	4.16	3.14	2.35	5.82	1.23	1.59	0.88	-0.04	1.24	3.39	2.27	1.00	0.46	4.19	0.34
MD-TC-6	5.23	6.91	3.46	3.81	3.47	3.40	4.18	3.23	2.45	5.78	1.30	1.69	0.92	-0.18	1.28	3.46	2.22	1.38	0.58	4.36	0.25
MD-TC-7	5.19	6.93	3.50	3.93	3.48	3.41	4.22	3.29	2.44	5.92	1.28	1.58	0.88	-0.12	1.28	3.59	2.23	0.95	0.57	4.49	0.28
MD-TC-8	5.20	6.88	3.52	3.84	3.49	3.43	4.23	3.33	2.47	5.95	1.30	1.58	0.90	-0.04	1.29	3.42	2.27	1.66	0.62	4.55	0.34
MD-TC-9	5.24	7.09	3.51	3.85	3.49	3.42	4.21	3.33	2.50	5.99	1.31	1.63	0.90	-0.25	1.28	3.63	2.19	1.05	0.59	4.31	0.27
MD-TC-10	5.00	7.01	3.40	3.72	3.37	3.29	4.13	3.13	2.40	5.88	1.13	1.52	0.78	-0.21	1.16	3.04	2.05	1.71	0.44	4.27	0.25
MD-TC-11	5.17	7.33	3.48	3.90	3.48	3.32	4.13	3.28	2.54	5.98	1.21	1.29	0.79	0.08	1.19	3.45	2.20	1.13	0.67	4.33	0.40
MD-TC-12	5.14	7.33	3.49	3.87	3.48	3.22	4.07	3.04	2.61	5.82	1.32	1.32	1.01	0.56	1.29	2.83	1.13	1.16	0.99	4.26	0.82
MD-TC-13	4.96	7.11	3.34	3.54	3.32	3.13	4.00	3.00	2.44	5.82	1.05	1.18	0.67	0.01	1.06	3.42	2.10	1.49	0.51	3.84	0.33
MD-TC-14	5.17	6.95	3.58	3.35	3.56	3.28	4.17	3.09	2.75	6.09	1.28	1.43	0.84	0.06	1.23	3.35	1.12	2.38	0.75	4.30	0.44
MD-TC-15	5.05	7.16	3.28	3.35	3.41	3.16	4.06	3.00	2.63	5.86	1.12	1.30	0.74	0.12	1.10	2.93	1.88	1.36	0.61	4.17	0.42
MD-TC-16	5.16	7.42	3.46	3.50	3.53	3.25	4.13	3.07	2.80	5.88	1.25	1.31	0.84	0.21	1.20	3.65	2.10	2.04	0.76	3.78	0.51
MD-TC-17	5.17	7.13	3.48	3.45	3.51	3.24	4.14	3.07	2.78	5.90	1.22	1.25	0.79	0.15	1.18	3.38	2.29	1.42	0.79	2.75	0.47
MD-TC-18	4.95	6.98	3.46	3.53	3.38	3.26	4.16	3.06	2.35	6.22	1.17	1.57	0.82	-0.22	1.19	3.37	2.19	2.84	0.40	4.28	0.28
MD-TC-19	5.26	6.83	3.68	3.67	3.60	3.51	4.35	3.15	2.50	6.27	1.47	1.61	0.98	-0.07	1.39	3.38	2.58	3.31	0.72	4.30	0.39
MD-TC-20	5.38	7.09	3.74	3.64	3.62	3.58	4.41	3.21	2.55	6.54	1.54	1.48	1.04	0.26	1.45	3.57	2.66	2.93	0.93	4.32	0.57
MD-TC-21	5.32	7.10	3.72	3.53	3.61	3.58	4.37	3.17	2.47	6.42	1.50	1.45	1.03	0.23	1.45	3.51	2.81	3.76	0.85	3.94	0.57
Median	5.19	7.05	3.48	3.72	3.48	3.40	4.18	3.15	2.47	5.88	1.30	1.46	0.90	0.01	1.28	3.42	2.19	1.49	0.63	4.30	0.39
Standard Deviation	0.12	0.21	0.11	0.20	0.08	0.14	0.10	0.11	0.13	0.23	0.13	0.15	0.10	0.21	0.11	0.22	0.40	0.82	0.16	0.42	0.14

Table B3: Trace element concentrations in surface water samples in recent studies in Southwest Bangladesh.

As[1]	**Cd**	**Cu**	**Cr**	**Fe**	**Mn**	**Ni**	**Pb**	**Zn**	**Months of sampling**	**Location**	**Study**
57.0	0.1	20.2	13.7	2.6	0.7	16.7	<MDL	16.5	May	Bhairab-Rupsha-Bhadra-Shibsa Rivers	This study
8.0				98.0					June-Aug	Ponds/Lakes in Rupsha Upazila	Ahmed et al. (2020)
3.5	6.5		45.2	976.6	288.5	18.7	18.4	68.4	March-May	Rupsha River Basin	Islam et al. (2020)
12.3	9.8		40.0	2062.0	65.4	21.4	26.6	33.8	March-May	Pasur River Basin	Islam et al. (2020)
5.5	1.0	5.4	7.2			3.9	7.1		Aug-Sept	Rupsha River	Proshad et al. (2020)
6.1	1.4	6.0	8.9			5.5	7.3		Jan-Feb	Rupsha River	Proshad et al. (2020)

[1]All concentrations are mean values, in µg/L.

References

Ahmed, A., Ghosh, P. K., Hasan, M., & Rahman, A. (2020). Surface and groundwater quality assessment and identification of hydrochemical characteristics of a south-western coastal area of Bangladesh. Environmental monitoring and assessment, 192(4), 1-15. https://doi.org/10.1007/s10661-020-8227-0

Dietrich, M., & Ayers, J. C. (2021). Influences on tidal channel and aquaculture shrimp pond water chemical composition in Southwest Bangladesh. *Geochemical Transactions*, 22(1), 1-22. https://doi.org/10.1186/s12932-021-00074-2

Gaillardet, J., Viers, J., Dupré, B. (2014). Trace Elements in River Waters in: Surface and Ground Water, Weathering and Soils, *Treatise on Geochemistry*. https://doi.org/10.1016/B978-0-08-095975-7.00507-6

Hale, R., Bain, R., Goodbred Jr., S., & Best, J. (2019). Observations and scaling of tidal mass transport across the lower Ganges–Brahmaputra delta plain: Implications for delta management and sustainability. *Earth Surface Dynamics*, *7*(1), 231–245. https://doi.org/10.5194/esurf-7-231-2019

Islam, A. R. M. T., Islam, H. T., Mia, M. U., Khan, R., Habib, M. A., Bodrud-Doza, M., ... & Chu, R. (2020). Co-distribution, possible origins, status and potential health risk of trace elements in surface water sources from six major river basins, Bangladesh. Chemosphere, 249, 126180. https://doi.org/10.1016/j.chemosphere.2020.126180

Mason, R. P. (2013). Trace metals in aquatic systems. John Wiley & Sons.

Proshad, R., Islam, S., Tusher, T. R., Zhang, D., Khadka, S., Gao, J., & Kundu, S. (2020). Appraisal of heavy metal toxicity in surface water with human health risk by a novel approach: a study on an urban river in vicinity to industrial areas of Bangladesh. Toxin Reviews, 1-17. https://doi.org/10.1080/15569543.2020.1780615